

A [2 × 2] nickel(II) grid and a copper(II) square result from differing binding modes of a pyrazine-based diamide ligand†

Julia Klingele (née Hausmann),^a John F. Boas,^b John R. Pilbrow,^b Boujemaa Moubaraki,^c Keith S. Murray,^c Kevin J. Berry,^d Keith A. Hunter,^a Geoffrey B. Jameson,^e Peter D. W. Boyd^f and Sally Brooker^{*a}

Received 11th October 2006, Accepted 28th November 2006

First published as an Advance Article on the web 14th December 2006

DOI: 10.1039/b614796h

The potentially bis-terdentate diamide ligand *N,N'*-bis[2-(2-pyridyl)ethyl]pyrazine-2,3-dicarboxamide (H_2L^{Et}) was structurally characterised. Potentiometric titrations revealed rather low pK_a values for the deprotonation of the first amide group of H_2L^{Et} (14.2) and *N,N'*-bis(2-pyridylmethyl)pyrazine-2,3-dicarboxamide (H_2L^{Me} , 13.1). Two tetranuclear copper(II) square complexes of H_2L^{Et} with a paddle-wheel appearance, in which each ligand strand acts as a linear N_3 –NO hybrid terdentate–bidentate chelate, have been isolated and structurally characterised. Complex $[Cu^{II}_4(H_2L^{Et})_2(HL^{Et})_2](BF_4)_6 \cdot 3MeCN \cdot 0.5H_2O$ ($3 \cdot 3MeCN \cdot 0.5H_2O$), with two nondeprotonated zwitterionic ligand strands and two monodeprotonated ligand strands, is formed in the 1 : 1 reaction of H_2L^{Et} and $Cu(BF_4)_2 \cdot 4H_2O$. It has a polymeric chain structure of tetranuclear subunits connected by $N-H \cdots N$ hydrogen bonds. The same reaction carried out with one equivalent of base gives the related compound $[Cu^{II}_4(HL^{Et})_4](BF_4)_4$ (**4**), with all four ligand strands monodeprotonated. It consists of isolated tetranuclear units. In both $3 \cdot 3MeCN \cdot 0.5 H_2O$ and **4** the copper(II) ions are in five-coordinate N_4O environments but the degree of trigonality (τ) differs [$3 \cdot 3MeCN \cdot 0.5H_2O$ $0.14 \leq \tau \leq 0.26$; **4** $\tau = 0.45$]. Under the same reaction conditions as for **4** but using $Ni(BF_4)_2 \cdot 6H_2O$ a tetranuclear [2 × 2] grid-type complex, $[Ni^{II}_4(HL^{Et})_4](BF_4)_4 \cdot 10H_2O$ (**5**·10 H_2O), is formed. The structure determination showed that the nickel(II) ions have N_6 distorted octahedral coordination spheres and all four ligand strands are monodeprotonated and act as N_3 – N_3 bis-terdentate chelates. Magnetic susceptibility data show that the complexes $3 \cdot 4H_2O$, **4** and **5**·10 H_2O exhibit very weak antiferromagnetic spin coupling. The energies and multiplicities of the spin states of $3 \cdot 4H_2O$ and **4** were determined from the temperature dependence of the magnetic susceptibility and indicate that a singlet state is lowest and the quintet state highest. This is consistent with the X-band EPR spectra of polycrystalline powders of $3 \cdot 4H_2O$ and **4**, measured down to 2.3 K, where the resonances observed at the lowest temperature are due to a triplet state. The *g*-values of the individual ions of **4** are consistent with the expected $d_{x^2-y^2}$ ground state for five-coordinate copper(II) in an approximately square pyramidal configuration.

Introduction

In recent years grid-type complexes and the self-assembly processes involved in their formation have attracted a considerable amount of interest.^{1–4} With typical octahedral metal ions like cobalt(II), iron(II), iron(III) or manganese(II) grid-type complexes

with intriguing electronic or magnetic properties have been reported.¹ For the formation of such grid-type complexes with octahedrally coordinated metal ions relatively rigid ligand systems with a repeating linear array of terdentate binding pockets are necessary. The use of amide-based ligands for the formation of grid-type complexes offers advantages over other systems since amides can usually be synthesised relatively easily. In addition to their good coordinating properties, amide groups also reduce the flexibility of a given ligand system.⁵

We recently reported that the use of a carefully designed amide-based ligand can also lead to pH control of product architecture.³ Specifically, that in MeCN solution the complexation of the potentially bis-terdentate diamide ligand *N,N'*-bis(2-pyridylmethyl)pyrazine-2,3-dicarboxamide (H_2L^{Me}) with $Cu(BF_4)_2 \cdot 4H_2O$ in a 1 : 1 molar ratio leads to the formation of a navy-blue cyclic dimeric complex $[Cu^{II}_2(H_2L^{Me})_2(MeCN)_2](BF_4)_4$ (**A**) of a zwitterionic form of H_2L^{Me} (Scheme 1).³ The ligand was thus shown to act as a hybrid N_3 –O terdentate–monodentate ligand, where one binding pocket is deactivated as a terdentate chelate by protonation of the pyridine nitrogen atom. It was also shown that under identical reaction conditions but with the

^aDepartment of Chemistry, University of Otago, PO Box 56, Dunedin, New Zealand. E-mail: sbrooker@alkali.otago.ac.nz; Fax: +64-3-479-7906; Tel: +64-3-479-7919

^bSchool of Physics, Building 27, Monash University, Clayton, Victoria, 3800, Australia

^cSchool of Chemistry, Building 23, Monash University, Clayton, Victoria, 3800, Australia

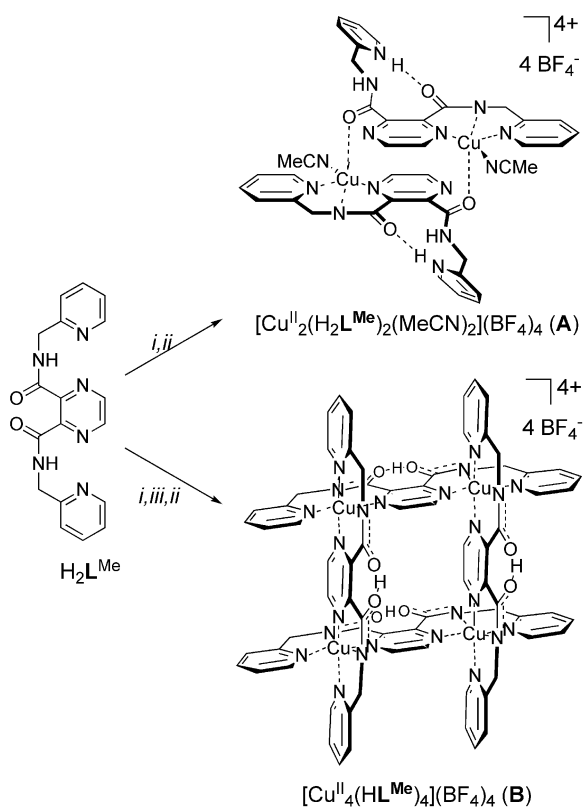
^dWesternport Secondary College, Hastings, Victoria, 3195, Australia

^eInstitute of Fundamental Sciences, Chemistry, Massey University, PO Box 11222, Palmerston North, New Zealand

^fDepartment of Chemistry, The University of Auckland, Private Bag 92019, Auckland, New Zealand

† Electronic supplementary information (ESI) available: A discussion of the IR data obtained for the complexes; magnetic data for complex **4** over the range 300–4.2 K (Fig. S1); crystallographic tables of selected bond lengths and angles and hydrogen-bonds (Tables S1–S3). See DOI: 10.1039/b614796h

addition of one equivalent of base, deprotonation of the pyridinium group occurs and that as a consequence the now monodeprotonated ligand ($\text{HL}^{\text{Me}}\text{)}^-$ acts as a bis-terdentate $\text{N}_3\text{-N}_3$ chelate. This results in the formation of a *grass-green* $[2 \times 2]$ grid-type complex $[\text{Cu}^{\text{II}}_4(\text{HL}^{\text{Me}})_4](\text{BF}_4)_4 \cdot 3.5\text{MeCN}$ (**B**) (Scheme 1).³ These two complexes, one a dimer, the other a tetranuclear grid, form due to a difference in the protonation state of the ligand, providing a nice illustration of the concept of using pH to control supramolecular architecture.^{3,6} Recently the synthesis⁴ and the crystal structures of an orthorhombic⁷ and a triclinic⁴ polymorph of $\text{H}_2\text{L}^{\text{Me}}$ were published by Stoeckli-Evans and co-workers, as were the syntheses, structures and magnetic properties of a copper(II) and a nickel(II) $[2 \times 2]$ grid-type complex $\{[\text{Cu}^{\text{II}}_4(\text{HL}^{\text{Me}})_4](\text{ClO}_4)_4 \cdot 5\text{MeOH} \cdot 4\text{H}_2\text{O}$ and $[\text{Ni}^{\text{II}}_4(\text{HL}^{\text{Me}})_4](\text{Cl})_4 \cdot 5\text{MeCN} \cdot 13\text{H}_2\text{O}$, respectively⁴ of $(\text{HL}^{\text{Me}})^-$.⁴ In contrast to the synthesis of **B** (Scheme 1), it is interesting to note that Stoeckli-Evans and co-workers used both a different anion (ClO_4^-) and a different solvent mixture ($\text{CH}_2\text{Cl}_2\text{-CH}_3\text{OH-H}_2\text{O}$) to prepare $[\text{Cu}^{\text{II}}_4(\text{HL}^{\text{Me}})_4](\text{ClO}_4)_4 \cdot 5\text{MeOH} \cdot 4\text{H}_2\text{O}$ and that under these conditions they did not require added base in order to form the $[2 \times 2]$ grid complex. This is a clear indication that a number of factors, including anion, solvent and probably also relative product solubilities, can influence the outcome of such complexations.



Scheme 1 Synthesis of **A** of the zwitterionic form of $\text{H}_2\text{L}^{\text{Me}}$ and of **B**, the $[2 \times 2]$ grid-type complex of $(\text{HL}^{\text{Me}})^-$. Reagents and conditions: (i) 1 eq. $\text{Cu}(\text{BF}_4)_2$, MeCN, RT; (ii) Et_2O (vapour diffusion); (iii) 1 eq. NEt_3 .

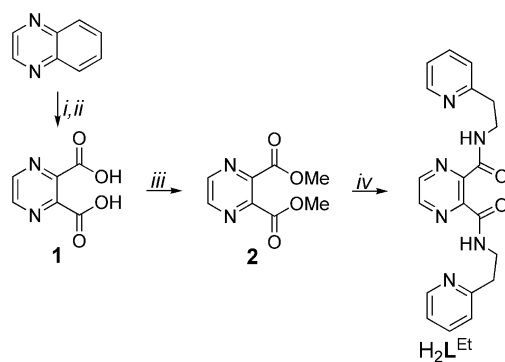
In this paper we report the results of our investigation into the effects of employing N,N' -bis[2-(2-pyridyl)ethyl]pyrazine-2,3-dicarboxamide ($\text{H}_2\text{L}^{\text{Et}}$),^{8,9} the higher homologue of $\text{H}_2\text{L}^{\text{Me}}$, on the molecular architecture of the resulting copper(II) and nickel(II) complexes. Specifically, as well as detailing a convenient new

synthesis of this ethylene-linked, potentially bis-terdentate, ligand ($\text{H}_2\text{L}^{\text{Et}}$), we report on its 1 : 1 reactions with $\text{Cu}(\text{BF}_4)_2 \cdot 4\text{H}_2\text{O}$ in MeCN, with and without base, for direct comparison with the results obtained for the methylene-linked ligand ($\text{H}_2\text{L}^{\text{Me}}$). It is clearly demonstrated that the change from methylene ($\text{H}_2\text{L}^{\text{Me}}$) to ethylene ($\text{H}_2\text{L}^{\text{Et}}$) 'arms' has a profound effect on the resulting copper(II) coordination environments as well as on the molecular architecture of the product formed. The synthesis and characterisation of a nickel(II) $[2 \times 2]$ grid-type complex of $(\text{HL}^{\text{Et}})^-$ is also described. Detailed magnetic susceptibility and EPR studies are also discussed.

Results and discussion

Ligand synthesis and pK_a studies

Dimethyl pyrazine-2,3-dicarboxylate (**2**) was conveniently prepared in a large scale in a one-pot two-step procedure by modification of the literature procedure (Scheme 2).¹⁰ The first step consisted of the oxidative cleavage of quinoxaline and the formation of pyrazine-2,3-dicarboxylic acid (**1**). In order to maximise the yield of diester **2**, the intermediate diacid **1** was not isolated. Instead the subsequent esterification with MeOH and SOCl_2 was carried out using the crude reaction product. The resulting diester **2** was easily isolated by extraction with CH_2Cl_2 and was obtained in very good yields as a slightly tan analytically pure crystalline solid. The ligand $\text{H}_2\text{L}^{\text{Et}}$ was prepared, by a modification of the literature procedure,⁸ by reacting dimethyl pyrazine-2,3-dicarboxylate (**2**) with 2-(2-aminoethyl)pyridine in a 1 : 2 molar ratio in MeOH in an open flask, thus allowing the MeOH formed in the reaction to evaporate. Redissolution of the remaining solid in $\text{CH}_2\text{Cl}_2\text{-Me}_2\text{CO}$ (2 : 1) and reduction of the volume of the solution afforded $\text{H}_2\text{L}^{\text{Et}}$ in very good yield as an analytically pure colourless microcrystalline solid (Scheme 2).



Scheme 2 Synthesis of $\text{H}_2\text{L}^{\text{Et}}$: Reagents and conditions: (i) KMnO_4 , H_2O , 80–90 °C; (ii) HCl (conc.), RT; (iii) SOCl_2 , MeOH, reflux; (iv) 2-(2-aminoethyl)pyridine, MeOH, open flask.

Owing to the apparent symmetry of $\text{H}_2\text{L}^{\text{Et}}$ the IR spectrum of the compound was expected to show only one band for the N–H and C–O stretching (ν_{NH} and ν_{CO}) vibrations as well as for the C–N stretching/N–H bending vibration ($\nu_{\text{C-N}}/\delta_{\text{NH}}$). In reality, two absorption bands for ν_{CO} ($\bar{\nu} = 1674$ and 1651 cm^{-1}) and $\nu_{\text{C-N}}/\delta_{\text{NH}}$ ($\bar{\nu} = 1541$ and 1509 cm^{-1}), were observed in the IR spectrum taken from a KBr disk. A similar observation was made by Stoeckli-Evans and co-workers for the IR spectrum of

the lower ligand homologue H_2L^{Me} ($\nu_{CO} : \bar{\nu} = 1676, 1665; \nu_{C-N}/\delta_{NH} : \bar{\nu} = 1534$ and 1515 cm^{-1}).⁴ The authors attributed this observation to different hydrogen bonding patterns exhibited by the two amide groups that were observed in the crystal structure of the triclinic polymorph of the free ligand, namely an intramolecular bifurcated hydrogen bond to a pyrazine and a pyridine nitrogen atom and an intermolecular hydrogen bond to the amide oxygen atom of a neighbouring ligand molecule.⁴

A single crystal X-ray structure analysis showed, however, that the molecular structure of H_2L^{Et} (Fig. 1) does not exhibit strong intramolecular hydrogen bonds but, more like the orthorhombic form of H_2L^{Me} ,⁷ that the two amide groups of H_2L^{Et} exhibit two different intermolecular hydrogen bonds $[N(2) \cdots N(3A) 3.165(3); N(5) \cdots O(2B) 2.825(3)]$ (Fig. 1). Owing to steric reasons, the *ortho*-positioned amide groups are not coplanar with each other or with the pyrazine ring. The mean planes defined by the amide functions $[O(1)-C(5)-N(2)$ and $O(2)-C(13)-N(5)]$ form angles of 19.5° and 52.6° to the pyrazine ring.

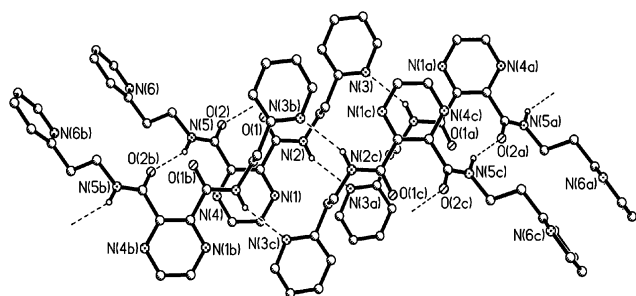


Fig. 1 Molecular structure of H_2L^{Et} . Hydrogen atoms not involved in hydrogen bonds have been omitted for clarity. Symmetry operation used to generate equivalent atoms: (a) $-x - 2, -y + 1, -z - 1$; (b) $x + 1, y, z$; (c) $-x - 1, -y + 1, -z - 1$.

For diamide derivatives of imidazole-4,5-dicarboxylic acid it is known that in the solid state generally an intramolecular $N-H \cdots O$ hydrogen bond motif is formed which leads to a seven-membered ring (motif **i** in Fig. 2).¹¹ In the IR spectra of some N,N' -disubstituted imidazole-4,5-dicarboxamides two ν_{CO} and two ν_{C-N}/δ_{NH} vibration absorption bands have been observed.¹² Although neither of the crystal structures of H_2L^{Me} ^{4,7} or H_2L^{Et}

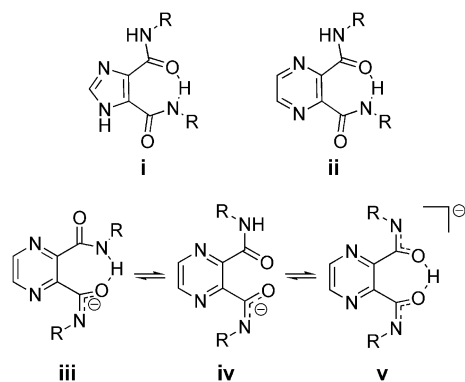


Fig. 2 **i**: Seven-ring motif found in diamide derivatives of imidazole-4,5-dicarboxylic acid; **ii**: seven-ring motif proposed for H_2L^{Me} and H_2L^{Et} in solution; **iii-v**: equilibria proposed for the monodeprotonated ligands $(HL^{Me})^-$ and $(HL^{Et})^-$ in solution.

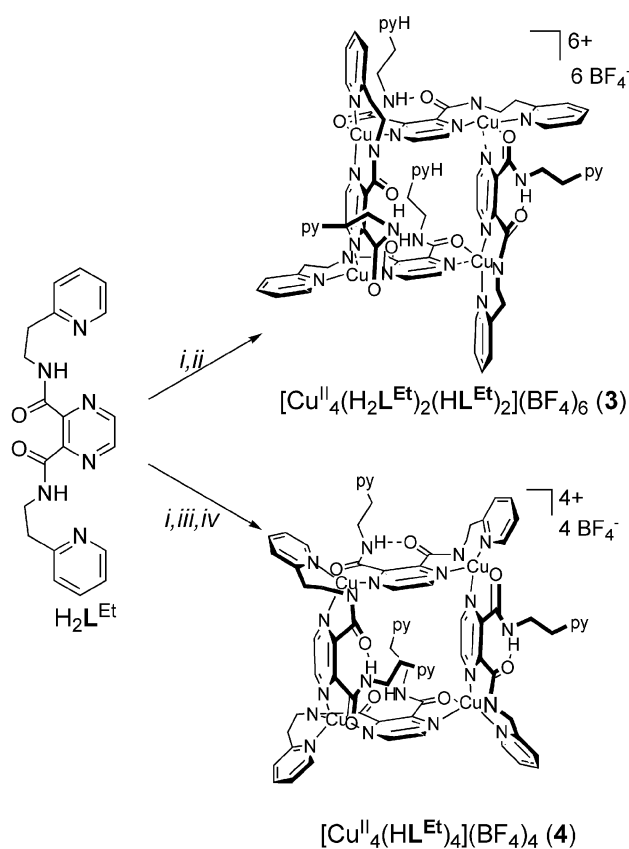
showed evidence of such a seven-membered ring in the solid state, a motif like **ii** in Fig. 2 is possible for the free ligand in solution.

The acid dissociation constants of both ligands, H_2L^{Me} and H_2L^{Et} , were measured by potentiometric titration with standard alkali solution using an established method.¹³ The method involved back titration of an aqueous solution containing known amounts of the ligand and standard aqueous hydrochloric acid with standard aqueous sodium hydroxide. It was assumed that each neutral ligand molecule contained two pyridine-N groups capable of accepting protons and a third functional group (amide) capable of losing a proton. The average computed first, second and third pK_a values, obtained from the non-linear fitting procedure, are $pK_1 = 4.4$ and 5.3 , $pK_2 = 5.2$ and 5.6 and $pK_3 = 13.1$ and 14.2 for H_2L^{Me} and H_2L^{Et} , respectively. The general magnitude of the pK_1 and pK_2 values for both ligands is consistent with the dissociation of isolated pyridinium protons ($pK_a = 5.23$ for the pyridinium ion at zero ionic strength).¹⁴ The much higher pK_3 values are likely to be due to the dissociation of an amide proton. Compared to the pK_a values of mono-amide compounds, which usually range from 16–19 (benzamide: $pK > 19$; acetanilide: $pK = 17.6$; benzanilide: $pK = 16.5$),¹⁵ the pK_3 values of 13.1 and 14.2 for the first amide group of H_2L^{Me} and H_2L^{Et} , respectively, are remarkably low. However, it is important to note that it is difficult to obtain accurate pK_a measurements at values greater than about 12 in aqueous media. The resulting monodeprotonated ligands $(HL^{Me})^-$ and $(HL^{Et})^-$ may be stabilised by the formation of equilibria involving motifs **iii-v** (Fig. 2). In $[2 \times 2]$ grid-type complexes of $(HL^{Me})^-$ seven-membered rings like motif **v** in Fig. 2 have been reported.^{3,4}

Synthesis and structures of tetranuclear copper(II) complexes

By analogy to the synthesis of $[Cu^{II}_2(H_2L^{Me})_2(MeCN)_2](BF_4)_4$ (**A**, Scheme 1)³ the 1 : 1 reaction of the higher ligand homologue H_2L^{Et} and $Cu(BF_4)_2 \cdot 4H_2O$ was carried out in MeCN solution (Scheme 3). Vapour diffusion of Et_2O into the resulting navy-blue solution afforded a compound formulated as $[Cu^{II}_2(H_2L^{Et})(HL^{Et})_n](BF_4)_{3n} \cdot 2nH_2O$, in *ca.* 85% yield, in the form of a turquoise-green crystalline material. In contrast to the zwitterionic form of H_2L^{Me} observed in the dimeric navy-blue complex **A**, in this tetranuclear turquoise-green complex only two of the ligand strands are in the zwitterionic form (H_2L^{Et}) whilst the other two are in a monodeprotonated form $(HL^{Et})^-$. The vapour diffusion of Et_2O into a dilute solution of the compound in MeCN afforded single crystals of $[Cu^{II}_4(H_2L^{Et})_2(HL^{Et})_2](BF_4)_6 \cdot 3MeCN \cdot 0.5H_2O$ (**3**: $3MeCN \cdot 0.5H_2O$) suitable for X-ray crystal structure analysis which revealed the tetranuclear nature of the compound ($n = 2$) and confirmed the form in which the ligands are present (Fig. 3, Tables 1 and S1–S3†).

Compound **3**: $3MeCN \cdot 0.5H_2O$ exhibits a square-like paddle-wheel structure built up by four copper(II) centres binding to the perpendicularly arranged portions of four ligand strands. The square encapsulates one tetrafluoroborate anion (Fig. 3). Each ligand acts as a linear N_3 -NO hybrid terdentate–bidentate chelate which results in an N_4O coordination sphere for each copper(II) centre with an average degree of trigonality¹⁶ of $\tau_{av} = 0.20$ ($0.14 \leq \tau \leq 0.26$). In the following discussion the coordination sphere will therefore be referred to as distorted square pyramidal. The central pyrazine rings of the ligands bridge adjacent copper(II)



Scheme 3 Synthesis of **3** and **4**: Reagents and conditions: (i) 1 eq. $\text{Cu}(\text{BF}_4)_2 \cdot 4\text{H}_2\text{O}$, MeCN, RT; (ii) Et_2O (vapour diffusion); (iii) 1 eq. NEt_3 , MeCN, RT; (iv) toluene (precipitation).

ions, occupying an equatorial and an apical position at each metal centre (see Scheme 3). In the square two shorter $[\text{Cu}(2) \cdots \text{Cu}(3)$ 6.997(1) Å and $\text{Cu}(3) \cdots \text{Cu}(4)$ 7.009(1) Å] and two slightly longer $[\text{Cu}(1) \cdots \text{Cu}(2)$ 7.051(1) Å and $\text{Cu}(1) \cdots \text{Cu}(4)$ 7.037(1) Å] Cu \cdots Cu distances are observed. In all four distorted square pyramids the copper(II) ions are pulled out of the base towards

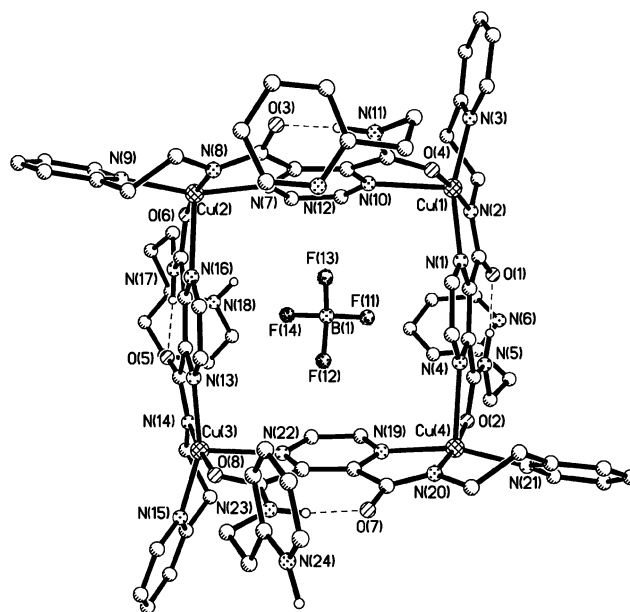


Fig. 3 Molecular structure of $[\text{Cu}^{\text{II}}_4(\text{H}_2\text{L}^{\text{Et}})_2(\text{HL}^{\text{Et}})_2]^{6+}$, the cation of 3-3MeCN-0.5H₂O, and its guest $(\text{BF}_4)^-$ anion. Hydrogen atoms except H(5C), H(11C), H(17C), H(23C) and the two pyridinium protons have been omitted for clarity.

the apical pyrazine ligand $[\text{Cu}(1): 0.165$ Å, $\text{Cu}(2): 0.162$ Å, $\text{Cu}(3): 0.157$ Å, $\text{Cu}(4): 0.127$ Å]. Relative to the Cu_4 mean plane, the copper(II) ions of the square are shifted by *ca.* 0.28 Å in an up-down-up-down fashion leading to a small tetrahedral distortion of the Cu_4 square.

Each *O*-coordinated amide group of the NO bidentate ligand half is still *N*-protonated. Within each ligand strand this proton is involved in an intramolecular $\text{N}-\text{H} \cdots \text{O}$ hydrogen bond to the oxygen atom of the *N*-metalated amide group of the N_3 terdentate half of the same ligand strand (Fig. 3). This motif is also present in the equilibria postulated for the metal-free monodeprotonated ligand (motif **iii** in Fig. 2) and is important as it enables the *ortho*-positioned amide groups, the deprotonated

Table 1 Comparison of selected bond distances [Å] and angles [°], and selected other data, for the complexes **A**, **B**, 3-3MeCN-0.5H₂O and **4**

	A ^a	B ^a	3-3MeCN-0.5H ₂ O ^a	4 ^a
Cu-L/Å				
Cu-N _{pz}	2.044(2)	2.171(9)–2.248(9)	2.027(5)–2.316(5)	2.024(6), 2.226(7)
Cu-N _{am}	1.913(2)	1.900(12)–2.002(11)	1.914(5)–1.931(5)	1.895(6)
Cu-O _{am}	2.270(1)	—	1.958(4)–1.997(4)	1.966(5)
Cu-N _{py}	2.017(2)	2.082(10)–2.194(10)	2.004(5)–2.027(5)	2.009(6)
L-Cu-L/°				
N _{py} -Cu-N _{am}	81.82(7)	77.2(3)–81.6(4)	93.7(2)–94.9(2)	93.9(3)
N _{py} -Cu-O _{am}	93.70(6)	—	91.4(2)–92.9(2)	92.0(2)
N _{py} -Cu-N _{pz}	162.85(6)	152.5(4)–157.0(4)	159.3(2)–163.7(2)	147.3(2)
O _{am} -Cu-N _{am} ^b	106.16(6) ^b	—	171.6(2)–174.9(2) ^b	174.0(3) ^b
O _{am} -Cu-N _{pz} ^a	—	—	73.2(2)–75.0(2) ^a	76.5(2) ^a
O _{am} -Cu-N _{py} ^b	92.22(6) ^b	—	90.9(2)–95.4(2) ^b	94.3(2) ^b
N _{am} -Cu-N _{pz}	81.08(6)	74.5(4)–76.8(4)	80.1(2)–80.8(2)	80.1(2)
Other data				
T/K	150	200	150	168
Structural type	Dimer	Tetramer; [2 × 2] grid-type	Tetramer; square	Tetramer; square
τ ²¹	0.05	Six-coordinate	0.14 ≤ τ ≤ 0.26	0.45

^a Only angles within the same ligand strand are given unless indicated otherwise. ^b Only angles between different ligands strands are given.

group of one *N*-metalated pocket and the nondeprotonated group of the other *O*-metalated pocket, to become coplanar. The $N \cdots O$ distances in the resulting seven-membered rings are in the range of 2.547–2.576 Å (Table S3) and are thus significantly shorter than those observed in related diamide derivatives of imidazole-4,5-dicarboxylic acid which usually are around 2.75–2.80 Å.¹¹ The *N*-metalated amide function is deprotonated and is part of the N_3 terdentate half of each ligand strand. In the tetrameric unit two of the four ligands are monodeprotonated $[(HL^{Et})^-]$ whereas the other two ligands are neutral (H_2L^{Et}). The latter are in a zwitterionic form, as the two former $N-H$ amide protons have relocated from the N_3 -terdentate half of each of these two ligands to protonate the uncoordinated pyridines of the NO-bidentate halves of each of these ligands. This feature has also been observed in the molecular structure of the related, but dimeric, complex **A** (Scheme 1) of the methylene ligand homologue and in other related systems.^{3,17} In **3** both relocated protons of the two H_2L^{Et} ligands are involved in intermolecular $N-H \cdots N$ hydrogen bonds to the two unprotonated pyridine nitrogen atoms of two $(HL^{Et})^-$ ligands in neighbouring tetranuclear subunits [2.703(5) Å and 2.732(5) Å]. In this way a polymeric chain of tetranuclear subunits is formed (Fig. 4). This was not a feature of the related dimeric complex **A** (Scheme 1).

There are many more differences between the complex of the ethylene linked ligand, $3 \cdot 3MeCN \cdot 0.5H_2O$ and the complex of the methylene linked ligand, **A**, not least the fact that **A** is dimetallic whereas $3 \cdot 3MeCN \cdot 0.5H_2O$ is tetrametallic. Both complexes contain distorted square pyramidal copper(II) centres but the basal plane in **A** comprises the N_3 terdentate chelate provided by H_2L^{Me} and an MeCN solvent molecule whereas in $3 \cdot 3MeCN \cdot 0.5H_2O$ it comprises the N_3 terdentate chelate provided by the higher ligand homologue H_2L^{Et} or $(HL^{Et})^-$ and an amide oxygen atom from a different ligand strand. The apical sites are also occupied by different groups, an amide oxygen atom from a different ligand strand in the case of **A** and a pyrazine nitrogen atom from the same ligand strand that provides the basal amide oxygen atom in the case of $3 \cdot 3MeCN \cdot 0.5H_2O$. In **A** one half of each ligand strand acts as an N_3 -terdentate chelate while the other half acts as a monodentate apical *O*-donor whereas in $3 \cdot 3MeCN \cdot 0.5H_2O$ one half of each ligand strand acts as an N_3 -terdentate chelate while the other half acts as an NO bidentate chelate which provides the remaining basal donor as well as the apical donor. These differences are presumably the result of the ethylene linked ligand modifying the

copper(II) coordination geometry (Table 1) by providing larger $N_{py}-Cu-N_{am}$ bite angles (six-membered chelate ring rather than five-membered chelate ring formed by the methylene linked ligand) and altering the preferred H-bonding patterns, favouring the intramolecular $N_{amide}-H \cdots O_{amide}$ hydrogen bonds between the *N*-protonated *O*-coordinated amide group in one half of the ligand and the oxygen atom of the *N*-metalated amide group in the other half of the same ligand strand as well as the intermolecular $N_{pyridine}-H \cdots N_{pyridine}$ hydrogen bonds between the pairs of protonated and unprotonated pyridine rings in neighbouring complexes, and associated solubility factors.

By analogy with the formation of **B** of the lower ligand homologue (Scheme 1), the 1 : 1 reaction of H_2L^{Et} with $Cu(BF_4)_2 \cdot 4H_2O$ in MeCN was repeated with the addition of one equivalent of base (Scheme 3) in order to ensure that all of the ligand strands are monodeprotonated so that both halves of each ligand strand are able, in principle, to act as N_3 terdentate chelates. A bottle-green amorphous solid formulated as $[Cu^{II}(HL^{Et})_n](BF_4)_n$ could be isolated, in excellent yield, from the resulting bottle-green solution by precipitation with toluene. The formula, proposed on the basis of elemental analysis results, clearly indicates that the strategy has been successful in producing a complex of monodeprotonated ligand strands $(HL^{Et})^-$ only. Vapour diffusion of Et_2O into a solution of the compound in MeCN afforded single crystals of $[Cu^{II}_4(HL^{Et})_4](BF_4)_4$ (**4**) suitable for an X-ray crystal structure determination (Fig. 5, Tables 1 and S1–S3†). This revealed the tetrameric nature of the compound ($n = 4$) and confirmed the presence of $(HL^{Et})^-$ ligands only, albeit binding in a very different manner to that observed in the analogous copper(II) complex **B** of $(HL^{Me})^-$.

The overall molecular structure of complex **4** is very similar to that of its precursor complex $3 \cdot 3MeCN \cdot 0.5H_2O$, again exhibiting a paddle-wheel appearance. A special position with $\bar{4}$ symmetry is located at the unoccupied centre of the tetranuclear square so the asymmetric unit comprises just a quarter of the tetramer, *i.e.* one $[Cu^{II}(HL^{Et})](BF_4)$ moiety. The ligand $(HL^{Et})^-$ in complex **4** acts as an N_3 -NO hybrid terdentate-bidentate chelate and, as seen in $3 \cdot 3MeCN \cdot 0.5H_2O$, this results in an N_4O five-coordinate copper(II) centre. The degree of trigonality ($\tau = 0.45$) is significantly higher than that of its precursor complex $3 \cdot 3MeCN \cdot 0.5H_2O$ ($\tau_{av} = 0.20$) and is between the values for a perfect square pyramid ($\tau = 0$) and a perfect trigonal bipyramid ($\tau = 1$).¹⁶ The $Cu \cdots Cu$ distance in this square [6.922(2) Å] is somewhat shorter

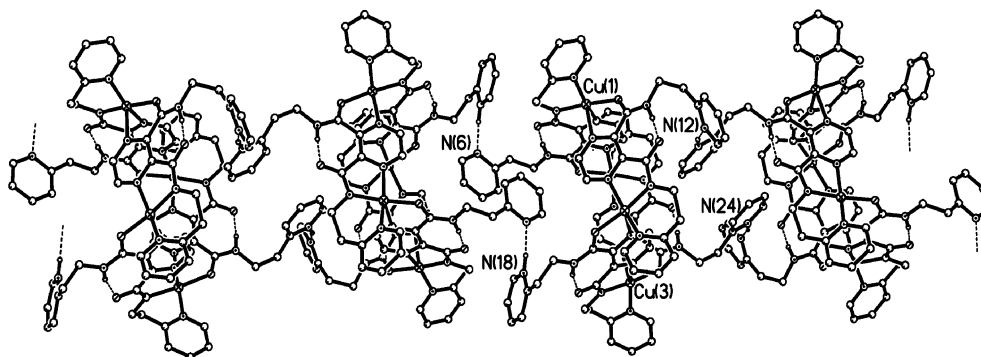


Fig. 4 Section of the polymeric chain structure of $3 \cdot 3MeCN \cdot 0.5H_2O$. Anions, solvent molecules and hydrogen atoms not involved in hydrogen bonds have been omitted for clarity.

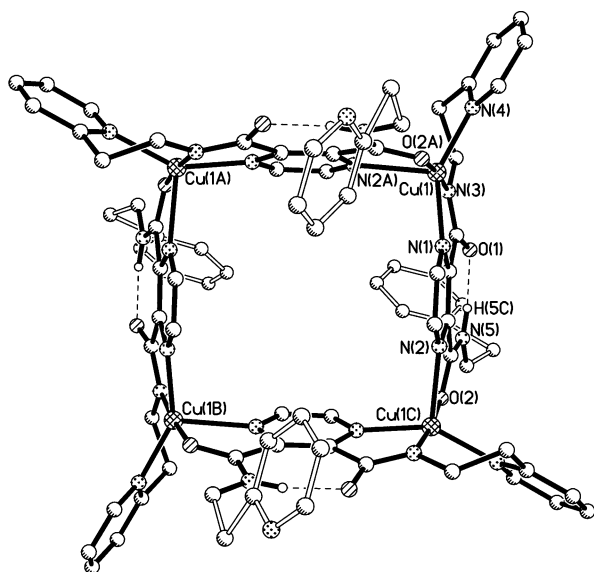


Fig. 5 Molecular structure of $[\text{Cu}^{\text{II}}_4(\text{HL}^{\text{Et}})_4]^{4+}$, the cation of **4**. Hydrogen atoms not involved in hydrogen bonds have been omitted for clarity. The hollow bonds denote the severely disordered free ligand arm, which was “SQUEEZEd away”¹⁸ in the refinement of the structure. Symmetry operations used to generate equivalent atoms: (A) $x - 0.5, -y + 0.5, -z + 0.5$; (B) $-x + 1, -y, z$; (C) $-x + 0.5, y + 0.5, -z + 0.5$.

than it is in $3\cdot 3\text{MeCN}\cdot 0.5\text{H}_2\text{O}$ (6.997–7.051 Å). Consistent with this, the copper(II) ions in **4** are shifted in an up–down–up–down fashion relative to the Cu_4 mean plane by a smaller amount (*ca.* 0.17 Å) than was observed in the case of $3\cdot 3\text{MeCN}\cdot 0.5\text{H}_2\text{O}$ (*ca.* 0.28 Å) and the $\text{Cu}-\text{N}_{\text{pz}}$ bonds, involved in the Cu –pyrazine– Cu bridges, are also slightly shorter in **4** (Table 1). As seen in the precursor complex $3\cdot 3\text{MeCN}\cdot 0.5\text{H}_2\text{O}$, each non-deprotonated amide function in complex **4** forms an intramolecular $\text{N}-\text{H}\cdots\text{O}$ hydrogen bond (Table S3), which leads to a seven-membered ring like motif **iii** in Fig. 2. Again, the pyridine ring of the bidentate ligand half points away from the square and is not coordinated to the copper(II) ion. However, in contrast to $3\cdot 3\text{MeCN}\cdot 0.5\text{H}_2\text{O}$, the uncoordinated pyridine nitrogen atom in **4** is not involved in intermolecular hydrogen bonding and is so disordered that it was subjected to the SQUEEZE procedure of the PLATON suite¹⁸ in order to complete the structural analysis.

To summarise, the addition of base to the 1 : 1 reaction of the ligand $\text{H}_2\text{L}^{\text{Et}}$ and $\text{Cu}(\text{BF}_4)_2\cdot 4\text{H}_2\text{O}$ turned the dark navy-blue solution bottle-green and led to the isolation of the bottle-green compound $[\text{Cu}^{\text{II}}_4(\text{HL}^{\text{Et}})_4](\text{BF}_4)_4$ (**4**) instead of the turquoise-green complex $[\text{Cu}^{\text{II}}_4(\text{H}_2\text{L}^{\text{Et}})_2(\text{HL}^{\text{Et}})_2](\text{BF}_4)_6\cdot 3\text{MeCN}\cdot 0.5\text{H}_2\text{O}$ ($3\cdot 3\text{MeCN}\cdot 0.5\text{H}_2\text{O}$). The structural consequences of removing the two pyridinium protons from $3\cdot 3\text{MeCN}\cdot 0.5\text{H}_2\text{O}$ to form **4** were subtle rather than dramatic as neither of the resulting pyridine nitrogen lone pairs coordinated to the copper(II) ions. Instead both $3\cdot 3\text{MeCN}\cdot 0.5\text{H}_2\text{O}$ and **4** contain four N_3 –NO coordinated copper(II) ions in a tetrameric square (Scheme 3). In stark contrast, in the analogous reaction with the methylene linked ligand $\text{H}_2\text{L}^{\text{Me}}$ the addition of base had dramatic structural consequences: the colour of the reaction solution changed from dark navy-blue to grass-green and the product isolated changed from the navy-blue dimer $\{[\text{Cu}^{\text{II}}_2(\text{H}_2\text{L}^{\text{Me}})_2(\text{MeCN})_2](\text{BF}_4)_4, \text{A}\}$ to the grass-green tetrameric $[2 \times 2]$ grid $\{[\text{Cu}^{\text{II}}_4(\text{HL}^{\text{Me}})_4](\text{BF}_4)_4\cdot 3.5\text{MeCN}, \text{B}\}$

(Scheme 1).³ The copper(II) ions in **A** are N_3 –NO coordinated whereas in **B** they are N_3 – N_3 coordinated. Complexes **B** and **4** are directly comparable to one another as they have the same $\text{Cu}(\text{II})$: ligand ratio and contain ligands in the same protonation state (monodeprotonated). It is therefore interesting to note that, despite these similarities, the copper(II) centres in **B** and **4** adopt differing coordination environments, N_3 – N_3 six-coordinate and N_3 –NO five-coordinate respectively, as a consequence of the difference in $\text{N}_{\text{py}}-\text{Cu}-\text{N}_{\text{am}}$ chelate ring sizes, five-membered and six-membered, offered by $(\text{HL}^{\text{Me}})^-$ and $(\text{HL}^{\text{Et}})^-$, respectively. In contrast, **A** and $3\cdot 3\text{MeCN}\cdot 0.5\text{H}_2\text{O}$ are not directly comparable. In this pair of complexes the $\text{Cu}(\text{II})$: ligand ratios are the same, but it is interesting to note that $3\cdot 3\text{MeCN}\cdot 0.5\text{H}_2\text{O}$ crystallises out with a mixture of monodeprotonated and non-deprotonated zwitterionic ligands whereas for the methylene linked analogue **A** the product contained only non-deprotonated zwitterionic ligands. Presumably this is a consequence of the relative solubilities of the various possible products in each case as much as their relative stabilities. In this context it is interesting to recall that $[2 \times 2]$ grids resulted from all of the following 1 : 1 complexations of $\text{H}_2\text{L}^{\text{Me}}$ (a) with copper(II) tetrafluoroborate in $\text{MeCN}-\text{Et}_2\text{O}$ when NEt_3 is added (Scheme 1, complex **B**)³ (b) with copper(II) perchlorate in $\text{CH}_2\text{Cl}_2-\text{MeOH}-\text{H}_2\text{O}$ with no added base⁴ and (c) with nickel(II) chloride in $\text{MeCN}-\text{MeOH}$ with NEt_3 added.⁴ It should also be noted that 1 : 2 reactions of $\text{H}_2\text{L}^{\text{Me}}$ or $\text{H}_2\text{L}^{\text{Et}}$ with copper(II) salts have consistently been reported to yield $\text{Cu}_2(\text{HL}^{\text{Me/Et}})_2\text{X}_3$ type species in the absence of added base. In 1974 Fleischer and co-workers⁹ reported the structure of $[\text{Cu}_2(\text{HL}^{\text{Me}})\text{Cl}_3]_{\infty}$, formed using copper(II) chloride in MeOH . More recently, again employing no added base, Stoeckli-Evans and co-workers⁴ reported the structure of $[\text{Cu}_2(\text{HL}^{\text{Me}})\text{Cl}_3(\text{H}_2\text{O})]$, formed using copper(II) chloride in $\text{EtOH}-\text{H}_2\text{O}$, and we have isolated $[\text{Cu}_2(\text{HL}^{\text{Me}})(\text{MeCN})_4](\text{BF}_4)_3$, using copper(II) tetrafluoroborate in $\text{MeCN}-\text{Et}_2\text{O}$. Taken together, these results clearly indicate that a great number of factors, including reaction stoichiometry, choice of anion and solvent(s), presence or otherwise of added base and the relative solubilities of the various possible products, all contribute, along with the exact nature of the ligand, to determining the nature of the complex isolated from these reactions.

Synthesis and structure of a tetranuclear nickel(II) complex

Employing similar reaction conditions to those employed in the synthesis of $3\cdot 3\text{MeCN}\cdot 0.5\text{H}_2\text{O}$ but replacing $\text{Cu}(\text{BF}_4)_2\cdot 4\text{H}_2\text{O}$ with $\text{Ni}(\text{BF}_4)_2\cdot 6\text{H}_2\text{O}$ led to a yellow-brown reaction mixture from which no well-defined product could be isolated. The addition of one equivalent of base to the reaction solution resulted in the isolation of the red-brown nickel(II) $[2 \times 2]$ grid-type complex $[\text{Ni}^{\text{II}}_4(\text{HL}^{\text{Et}})_4](\text{BF}_4)_4\cdot 10\text{H}_2\text{O}$ (**5**· $10\text{H}_2\text{O}$) of monodeprotonated ligands $(\text{HL}^{\text{Et}})^-$. Single crystals of **5**· 10MeCN suitable for X-ray crystal structure determination were obtained by vapour diffusion of Et_2O into a MeCN solution of the compound (Fig. 6, Tables 2 and S1–S3†).

In contrast to the tetracopper(II) complex **4**, in the tetranickel(II) complex **5**· 10MeCN the monodeprotonated ligands act as N_3 – N_3 bis-terdentate chelates. The equatorial N_3 coordination of two approximately perpendicular binding pockets results in N_6 distorted octahedral coordination spheres for the nickel(II) ions. The

Table 2 Comparison of selected bond distances [Å] and angles [°], and selected other data, for the complexes **5**·10MeCN and $[\text{Ni}^{\text{II}}_4(\text{HL}^{\text{Me}})_4](\text{Cl})_4 \cdot 5\text{MeCN} \cdot 13\text{H}_2\text{O}^{\text{a}}$

	5 ·10MeCN ^a	$[\text{Ni}^{\text{II}}_4(\text{HL}^{\text{Me}})_4](\text{Cl})_4 \cdot 5\text{MeCN} \cdot 13\text{H}_2\text{O}^{\text{a}}$
<i>Ni-L/A</i>		
Ni–N _{pz}	2.104(5)–2.174(4)	2.107(5)–2.131(5)
Ni–N _{am}	2.017(5)–2.047(4)	1.979(4)–2.000(4)
Ni–N _{py}	2.042(4)–2.163(4)	2.065(4)–2.094(4)
<i>L–Ni–L/°</i>		
N _{py} –Ni–N _{am}	90.6(2)–93.1(2)	79.2(2)–79.9(2)
N _{py} –Ni–N _{pz}	165.3(2)–169.4(2)	155.7(2)–156.9(2)
N _{am} –Ni–N _{pz}	75.6(2)–77.4(2)	76.4(2)–77.0(2)
<i>Other data</i>		
T/K	150	153
Structural type	Tetramer; [2 × 2] grid-type	Tetramer; [2 × 2] grid-type

^a Only angles within the same ligand strand are given.

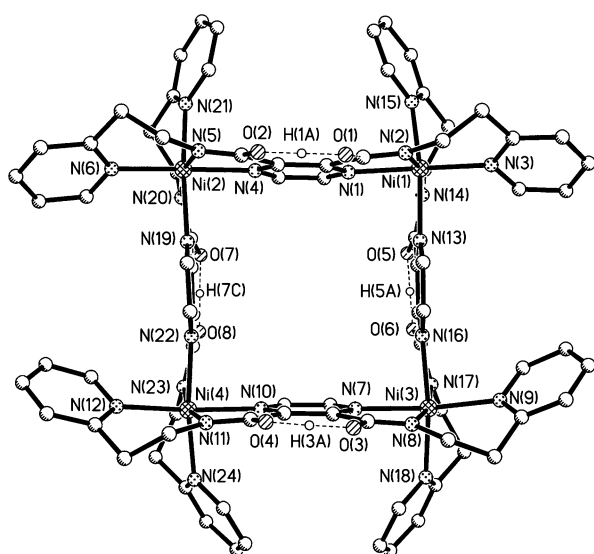


Fig. 6 Molecular structure of $[\text{Ni}^{\text{II}}_4(\text{HL}^{\text{Me}})_4]^{4+}$, one of the two cations present in the asymmetric unit of **5**·10MeCN. Hydrogen atoms not involved in hydrogen bonds are omitted for clarity.

asymmetric unit contains two crystallographically independent grid cations. As in the square compounds **3**·3MeCN·0.5H₂O and **4** the pairs of immediately adjacent amide groups in **5**·10MeCN are arranged in a coplanar fashion. However, in contrast to the copper(II) complexes **3**·3MeCN·0.5H₂O and **4** where the coplanarity was achieved by N–H···O hydrogen bonding between these amide moieties, in the case of this nickel(II) complex the coplanarity is achieved by intramolecular O···H···O hydrogen bonds between these amide moieties (Table S3). Similar [2 × 2] grid-type copper(II)^{3,4} and nickel(II)⁴ complexes of the mono-deprotonated lower ligand homologue (HL^{Me})[–] also contained O···H···O hydrogen bonds and such a species is part of the equilibrium postulated for the monodeprotonated free ligand (HL^{Et})[–] (motif **v** in Fig. 2).

The Ni–N distances in this ethylene linked [2 × 2] grid-type complex **5**·10 MeCN are broadly similar to those in the related methylene linked [2 × 2] grid-type complex $[\text{Ni}^{\text{II}}_4(\text{HL}^{\text{Me}})_4](\text{Cl})_4 \cdot 5\text{MeCN} \cdot 13\text{H}_2\text{O}$ described earlier by Stoeckli-Evans⁴ (Table 2). However, it is interesting to note that the Ni–N_{am} bonds in the methylene linked analogue [1.979(4)–1.999(4) Å]⁴ are all slightly

shorter than those observed in the ethylene linked analogue **5** [2.017(5)–2.047(4) Å]. Given that the amide nitrogen atom is the central donor atom of the approximately planar N₃-chelate, this allows the N_{am}–Ni–N_{py} bond angle in these five-membered chelate rings in $[\text{Ni}^{\text{II}}(\text{HL}^{\text{Me}})]_4^{4+}$ to open up somewhat [79.2(2)–79.9(2)°],⁴ although they are still rather small for a six-coordinate first row transition metal ion, especially when compared to the same angle in the six-membered chelate rings in the ethylene linked analogue **5** [90.6(2)–92.6(2)°]. In contrast, in both of these complexes the N_{pz}–M–N_{am} angles of the N₃-chelate are contained within rather rigid five-membered chelate rings so are similar to one another, although a slightly wider range of angles is observed for the ethylene linked complex **5** [76.4(2)–77.0(2)° for $[\text{Ni}^{\text{II}}(\text{HL}^{\text{Me}})]_4^{4+}$ vs 75.6(2)–77.4(2)° for **5**].

Magnetic and EPR studies

The temperature dependence of the magnetic susceptibility was measured for the complexes **3**·4H₂O, **4** and **5**·10H₂O. The plots of μ_{eff} and χ_{m} , per Cu (or Ni), versus *T* for the compounds **3**·4H₂O and **5**·10H₂O are given in Fig. 7 and 8 while that for **4** is given in

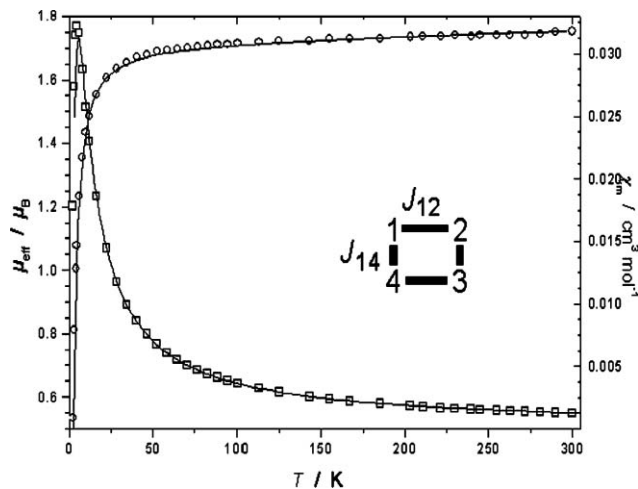


Fig. 7 Thermal variation of μ_{eff} (○) and χ_{m} (□), per copper(II), for $[\text{Cu}^{\text{II}}_4(\text{H}_2\text{L}^{\text{Et}})_2(\text{HL}^{\text{Et}})_2](\text{BF}_4)_6 \cdot 4\text{H}_2\text{O}$ (**3**·4H₂O). The solid lines represent the best fits (see text). Inset: Tetranuclear arrangement of the copper(II) centres in **3**·4H₂O.

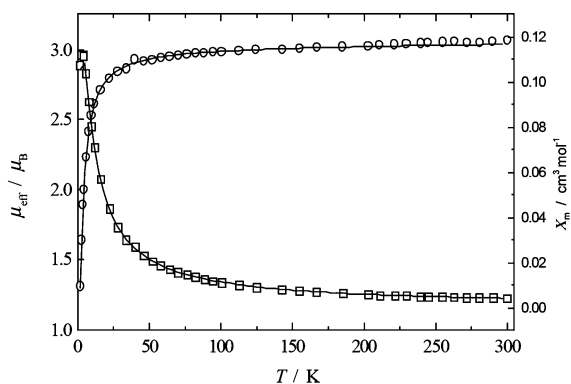


Fig. 8 Thermal variation of μ_{eff} (○) and χ_m (□), per nickel(II), for $[\text{Ni}^{\text{II}}_4(\text{HL}^{\text{Et}})_4](\text{BF}_4)_4 \cdot 10\text{H}_2\text{O}$ ($5 \cdot 10\text{H}_2\text{O}$). The solid lines represent the best fits.

Fig. S1.† Observations of maxima in the magnetic susceptibility measurements at very low temperatures for the tetranuclear copper(II) complexes $3 \cdot 4\text{H}_2\text{O}$ and **4** and the nickel(II) complex, $5 \cdot 10\text{H}_2\text{O}$, indicated very weak antiferromagnetic coupling.

The magnetic data for the two copper(II) tetranuclear clusters were fitted to a model^{19,20} that uses the numbering scheme shown in Fig. 3 and 7 (inset) and the exchange Hamiltonian (eqn (1)), in which the $2J_{13}$ cross (diagonal) term was set at zero;

$$H = -2J_{12}(\mathbf{S}_1 \cdot \mathbf{S}_2 + \mathbf{S}_3 \cdot \mathbf{S}_4) - 2J_{14}(\mathbf{S}_1 \cdot \mathbf{S}_4 + \mathbf{S}_2 \cdot \mathbf{S}_3) - 2J_{13}(\mathbf{S}_1 \cdot \mathbf{S}_3 + \mathbf{S}_2 \cdot \mathbf{S}_4) \quad (1)$$

A full matrix diagonalisation of the 16×16 matrix was also carried out that confirmed the J values and yielded the energies of the coupled states, S , used below in the EPR discussion. The best-fit to this tetranuclear $S = 1/2$ model was obtained with $J_{12} = -1.9 \pm 0.1 \text{ cm}^{-1}$, $J_{14} = -2.4 \pm 0.1 \text{ cm}^{-1}$, $g = 1.99 \pm 0.01$, $\text{TIP} = (65 \pm 5) \times 10^{-6} \text{ cm}^3 \text{ mol}^{-1}$ [per copper(II)] and % monomer = 0.1 for compound $3 \cdot 4\text{H}_2\text{O}$. This was a markedly improved fit compared to using a single J value. The g value is a little low for copper(II) but it essentially reflects the room temperature value of μ_{eff} , per copper(II), being close to the spin-only value for d^9 . It is lower than the value obtained from the powder EPR spectrum (*vide infra*), but this is not uncommon in fitting of susceptibilities when allowing parameters to refine to the best fit. The small J values obtained from the fitting procedure are anticipated for a tetranuclear system having pyrazine bridging along each side of the distorted square since pyrazine is known to yield a poor antiferromagnetic exchange pathway when bridging copper(II) ions. Furthermore, each pyrazine moiety binds in an equatorial-axial manner to adjacent copper(II) atoms (Fig. 3). Thus the mutual orthogonality of the $d_{x^2-y^2}$ ‘magnetic’ orbitals on adjacent copper(II) centres will provide a ferromagnetic contribution to the net coupling and lead to the small negative J values obtained. The distortions of the copper(II) coordination geometries towards trigonal bipyramidal will further cause a diminution in resultant J values. The H-bonded amide pathways are not likely to contribute significantly to the J values. The small differences in J_{12} and J_{14} probably reflect differences noted in $\text{Cu} \cdots \text{Cu}$ edge separations even though the adjacent edges are of rather similar separation, *i.e.* $\text{Cu}(1) \cdots \text{Cu}(2) \approx \text{Cu}(1) \cdots \text{Cu}(4) > \text{Cu}(3) \cdots \text{Cu}(4) \approx \text{Cu}(2) \cdots \text{Cu}(3)$.

For the complexes **4** and $5 \cdot 10\text{H}_2\text{O}$, it was found that $J_{12} = J_{14} = J$, in agreement with the very similar $\text{M} \cdots \text{M}$ distance obtained from crystallography, and thus one value for J (-3.02 ± 0.02 and $-0.80 \pm 0.02 \text{ cm}^{-1}$, respectively) yielded the best fit, together with the following parameters: $g = 2.07 \pm 0.01$, 2.14 ± 0.01 ; $\text{TIP} = (65 \pm 5) \times 10^{-6}$, $(100 \pm 5) \times 10^{-6} \text{ cm}^3 \text{ mol}^{-1}$, per $\text{M}(\text{II})$, % monomer = 0.1, 0 for the complexes **4** and $5 \cdot 10\text{H}_2\text{O}$, respectively. An $S = 1$ cycle square model was used for the nickel(II) complex $5 \cdot 10\text{H}_2\text{O}$ ^{20,21} and the zero-field splitting term D was assumed to be zero. Perusal of the value of χ_m at the maximum ($0.114 \text{ cm}^3 \text{ mol}^{-1}$), and comparing it to the plateau value expected in distorted octahedral nickel(II) species having zero field splitting with no exchange coupling,²² suggests an approximate value of $|D|$ of $\sim 2 \text{ cm}^{-1}$. We note that J values of -2.93 cm^{-1} and -1.32 cm^{-1} were obtained for the related complexes $[\text{Cu}^{\text{II}}_4(\text{HL}^{\text{Me}})_4](\text{ClO}_4)_4 \cdot 5\text{MeOH} \cdot 4\text{H}_2\text{O}$ and $[\text{Ni}^{\text{II}}_4(\text{HL}^{\text{Me}})](\text{Cl})_4 \cdot 5\text{MeCN} \cdot 13\text{H}_2\text{O}$, respectively,⁴ in very good agreement with the present results for the HL^{Et} compounds.

The multiplicities and relative energies of the spin states in zero field can be obtained directly through matrix diagonalization of the exchange Hamiltonian (eqn (1)) or from published equations.²³ For the ‘magnetically rectangular’ complex $3 \cdot 4\text{H}_2\text{O}$ ($J_{12} \neq J_{14}$, $J_{13} = 0$) we obtain a ground singlet state, triplet states at 4.5 cm^{-1} and 8.6 cm^{-1} , a singlet state at 9.0 cm^{-1} , a triplet state at 9.3 cm^{-1} and a quintet state at 13.4 cm^{-1} . For the ‘square’ complex **4** ($J_{12} = J_{14}$, $J_{13} = 0$) we obtain a ground singlet state, a triplet state at 6.04 cm^{-1} , two triplet states and a singlet state at 12.08 cm^{-1} and a quintet state at 18.12 cm^{-1} . These spin state multiplicities and energies do not take account of the admixture of states from closely spaced multiplets in applied magnetic fields or of small zero field splittings within triplet and quintet states due to second order exchange (possibly $\sim 0.01 \text{ cm}^{-1}$) and dipole-dipole interactions (for copper(II) ions approximately 7 \AA apart estimated as $\sim 0.005 \text{ cm}^{-1}$).

The EPR spectrum of a polycrystalline powder of $3 \cdot 4\text{H}_2\text{O}$ was recorded at X-band frequencies ($\sim 9.5 \text{ GHz}$) at temperatures from 295 K down to 2.5 K . As shown in Fig. 9 it exhibited an intense almost isotropic resonance at $g \sim 2.10$ whose derivative peak to peak width of around 150 G was independent of temperature.

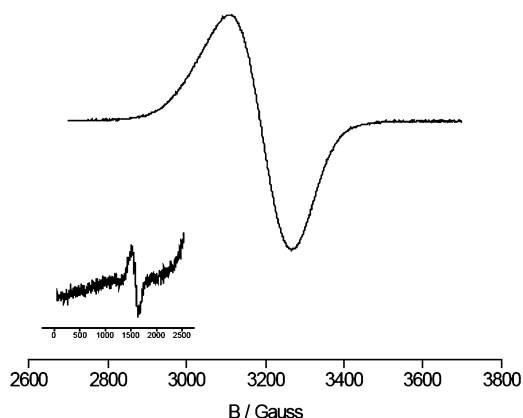


Fig. 9 EPR spectrum of $3 \cdot 4\text{H}_2\text{O}$ at 9.435 GHz and 110 K . Main spectrum ($g = 2$ region): Spectrometer gain 4.0×10^3 , microwave power 1.05 mW , 100 kHz modulation amplitude 1.0 G , scan time 84 s , time constant 41 ms . Inset of low field region (including $g = 4$ region): Spectrometer gain 2.0×10^5 , microwave power 5.26 mW , 100 kHz modulation amplitude 5.0 G , scan time 84 s , time constant 41 ms .

Another isotropic resonance of width 120 G was observed at $g \sim 4.2$ at 1000 times the spectrometer gain at 295 K and 110 K (inset, Fig. 9), but there was no clear evidence for its presence at 2.5 K. No other resonances were observed at any temperature over the field range from 0 to 8000 G. The X-band EPR spectra of a polycrystalline powder of **4** at 295 K and 2.3 K are shown in Fig. 10 (solid lines), where the changes in appearance of the spectra are due to an increased linewidth and a decreased g value for the higher field region at 2.3 K. No other resonances were observed in the range from zero field to 8000 G, specifically near $g = 4$, at any temperature.

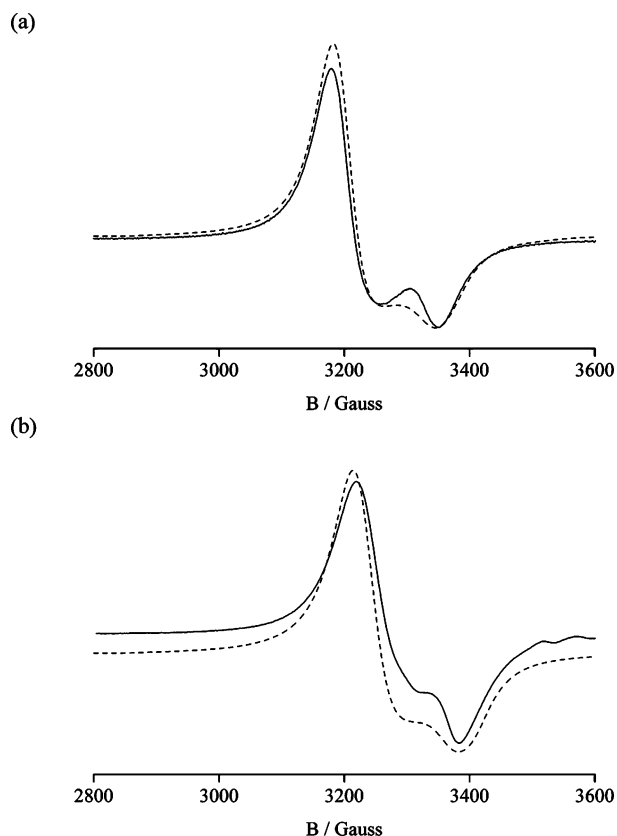


Fig. 10 EPR spectra of **4**. Full line: experimental spectra; broken lines: simulated spectra using parameters as in Table 3. (a) Experimental spectrum at 295 K, microwave frequency 9.623 GHz, spectrometer gain 1.0×10^3 , microwave power 1.05 mW, 100 kHz modulation amplitude 0.5 G, scan time 84 s, time constant 41 ms. Simulated spectrum: $S = 2$. The simulated spectrum for $S = 1$ is identical. (b) 2.3 K, microwave frequency 9.695 GHz, spectrometer gain 4.0×10^3 , microwave power 1.05 mW, 100 kHz modulation amplitude 1.0 G, scan time 84 s, time constant 41 ms. Simulated spectrum: $S = 1$.

On first inspection, both spectra have the appearance of arising from a simple $S = 1/2$ system. Indeed, EPR spectra with a superficial similarity to that of **4** have been attributed to copper(II) ions subjected to fluxional Jahn–Teller distortions²⁴ or in a d_{z^2} ground state.²⁵ In the present case, the essentially temperature independent appearance of both spectra from room temperature down to below 3 K contra-indicates these interpretations. More importantly, interpretations in terms of total spin $S = 1/2$ systems are clearly untenable given the tetranuclear configuration of these complexes and the EPR spectral features must arise from

Table 3 Spin Hamiltonian parameters: g values, spin state multiplicities (S) and zero-field splitting parameters (D) and line widths for the simulated spectra of **4** shown in Fig. 10. The copper(II) hyperfine interaction has been set to zero, as it is assumed to be averaged out by the exchange interactions

T/K	g_{\parallel}	g_{\perp}	S	$D/10^{-4} \text{ cm}^{-1}$	$\sigma_{\parallel}/10^{-4} \text{ cm}^{-1}$	$\sigma_{\perp}/10^{-4} \text{ cm}^{-1}$
295.0	2.048	2.150	1	15	37	42
295.0	2.048	2.150	2	7	37	42
2.3	2.042	2.143	1	15	37	47

transitions between levels within the triplet ($S = 1$) and quintet ($S = 2$) states. The present complexes are similar to some other tetranuclear grid-like copper(II) complexes,^{26–28} although in the present case, the exchange interactions are an order of magnitude or more smaller. This means that the zero-field splittings of the triplet and quintet states due to second order exchange and dipolar interactions between the copper(II) ions will be quite small and not resolved if they are less than the component line widths. Furthermore, it can be shown that since the directions of the x , y and z axes of the g matrices of the individual ions are the same, the components of the g matrices of each of the multiplets will be the same.^{26,27} Thus the question of whether the resonances arise from transitions within triplet and/or quintet states cannot be resolved from the appearance of the spectra alone, but requires a detailed analysis of the temperature dependence of the resonance intensities. Although a detailed analysis was not performed, a comparison of the spectral intensities at 4.3 K and 2.5 K for **3·4H₂O** and at 3.3 K and 2.3 K for **4**, combined with the relative population of each of the spin multiplets and the application of the Boltzmann $1/T$ factor to the states within each multiplet, leads to the conclusions, consistent with the magnetic susceptibility results, that both complexes have a $S = 0$ (singlet) state lowest in energy with the resonances observed in the 4 K region arising almost completely from the lowest triplet level. At temperatures much above 50 K, the spin states are populated very closely according to their multiplicity and presumably the other two triplet states and the quintet state contribute to the EPR spectral intensity. As shown by the broken lines in Fig. 10a and 10b, the spectra of **4** can be adequately simulated assuming either triplet or quintet states and the parameters listed in Table 3. The simulations of Fig. 10 included a small zero-field splitting term, D , in the spin Hamiltonian, where the value of D given in Table 3 was the largest that did not have a significant effect on the spectrum.

The relationship between the EPR spectra of the tetranuclear cluster as a whole and that expected from the individual copper(II) ions can be understood by an extension of the argument of Mann *et al.* as follows.²⁸ Each copper(II) ion in both **3·4H₂O** and **4** may be visualised as lying near the centre of the base of an approximately square pyramidal arrangement. Using Cu(1) in **3·4H₂O** as an example, we see that O(4), N(1), N(2) and N(3) form the base for Cu(1) and N(10) is in the apical position. Although the g matrix axes of Cu(1) need not closely coincide with the bond directions, it is reasonable to propose that g_z lies along the Cu(1)⋯N(10) direction (the longest bond distance 2.316 Å) and that g_x and g_y are closely similar in magnitude and lie close to the plane containing O(4), N(1), N(2) and N(3) with bond distances between 1.91 Å and 2.032 Å respectively. Further, we may define the direction of g_x as being close to that of the bond Cu(1)⋯O(4), leaving the bond direction of Cu(1)⋯N(1) to define the direction of

g_y . An analogous argument applies to the other three copper(II) ions of **3**·4H₂O and to the four copper(II) ions of **4**. Since the + and – directions are indistinguishable by EPR, directions such as those of Cu(1)···O(4) and Cu(1)···N(2) can be regarded as magnetically equivalent. Similar considerations apply to **4**.

Considering the tetranuclear structure as a whole, we see that the bond directions equivalent to Cu(1)···O(4) and hence the directions of g_x of the individual ions are approximately parallel for all four copper(II) ions, point out of the plane of the copper(II) grid and become the *de-facto* g_{\parallel} principal direction. Furthermore, the directions of g_y and g_z are rotated by 90° around g_x as we progress around the sides of the grid, establishing the conditions for anti-symmetric exchange coupling in two dimensions between magnetically inequivalent sites, analogous to that occurring in some CuCl₄²⁻ complexes.²⁹

In the case of **3**·4H₂O the absence of features due to anisotropic g values, copper(II) hyperfine structure and splittings due to second order exchange and dipolar interactions suggests that the exchange interactions are such that all anisotropic interactions are collapsed into a single isotropic line. The exchange averaged g value of 2.10 (±0.01) can be obtained from g values of the individual ions consistent with the range of expectation for a $d_{x^2-y^2}$ ground state for five-coordinate copper(II), namely $g_{\parallel} \sim 2.24$ and $g_{\perp} \sim 2.03$. One dimensional intermolecular exchange evidenced by the observation of the $g \sim 4$ resonance and attributed to the N–H···N hydrogen bonds linking the polymeric chain structure of tetranuclear subunits (see above and Table S3) may well make a contribution to the exchange averaging at higher temperatures.²⁶ The disappearance of the resonance at $g \sim 4.2$ at very low temperatures could be due to the depopulation of the higher lying multiplets and consequent reduction in this contribution.

In the case of **4**, the apparent reversal of the g values can be explained if exchange averaging occurs between the ions of the grid along the y and z axes to give an exchange averaged peak with a g value of $1/2(g_y + g_z)$. Since this peak is the accumulation of intensity when the magnetic field is in the $y - z$ plane, it will have a greater intensity than the peak corresponding to g_x and thus give a perpendicular appearance. We then can identify the “parallel” peak at $g \approx 2.05$ with g_x and the “perpendicular” peak at $g \approx 2.15$ with $1/2(g_y + g_z)$. If $g_x = g_y = 2.05$, we obtain $g_z = 2.25$, leading to single copper(II) ion values of $g_{\parallel} = 2.25$ and $g_{\perp} = 2.05$, consistent with the expected $d_{x^2-y^2}$ ground state for five-coordinate copper(II) in an approximately square pyramidal configuration. This is also consistent with coordination to N₃O₁ in a square planar environment.³⁰ A further effect of the exchange averaging is to smear out both the hyperfine interactions of each of the copper(II) ions and the small zero-field splittings arising from second order exchange and dipolar interactions between the copper(II) ions.

Although inter- and intra-molecular interactions may be delineated through a comparison of the spectra of powders and frozen solutions, both these tetranuclear complexes appear to form solute aggregates in the more concentrated frozen solutions of less aggressively coordinating solvents such as MeCN and MeOH and disintegrate in dilute solution and in the more strongly coordinating solvents such as DMF. A frozen solution of **4** in DMF exhibited a monomeric copper(II) spectrum with $g_{\parallel} = 2.240$ and $g_{\perp} = 2.059$, together with superhyperfine structure consistent with coordination by three N atoms. These g values are consistent with the analysis of the powder spectrum described above.

Conclusions

The potentially bis-terdentate diamide ligand *N,N'*-bis[2-(2-pyridyl)ethyl]pyrazine-2,3-dicarboxamide (H₂L^{Et}) has been structurally characterised. Potentiometric titrations carried out on *N,N'*-bis(2-pyridylmethyl)pyrazine-2,3-dicarboxamide (H₂L^{Me}) and H₂L^{Et}, revealed rather low p*K*_a values for the deprotonation of the first amide group. This was tentatively attributed to the possible formation of equilibrium structures, which could stabilise the monodeprotonated species and at the same time enable the amide groups to become coplanar.

Tetracopper(II) complexes with paddle-wheel square-like structures, [Cu^{II}₄(H₂L^{Et})₂(HL^{Et})₂](BF₄)₆ (**3**) and [Cu^{II}₄(HL^{Et})₄](BF₄)₄ (**4**), have been obtained by the 1 : 1 reaction of ligand H₂L^{Et} and Cu(BF₄)₂·4H₂O, without and with the addition of one equivalent of base, respectively. In both complexes the ligands act as hybrid NO–N₃ bidentate–terdentate chelates, resulting in N₄O coordination spheres about the copper(II) ions. The most pronounced differences between the tetrameric cations of **3** and **4** are observed in the five-coordinate copper(II) coordination spheres ($\tau_{av} = 0.20$ versus $\tau = 0.45$) and the fact that in compound **3** the ligand exists as monodeprotonated ligand (HL^{Et})⁻ as well as neutral zwitterionic ligand H₂L^{Et}, whereas in complex **4** solely monodeprotonated ligand (HL^{Et})⁻ is present. The change from methylene (H₂L^{Me}) to ethylene (H₂L^{Et}) ligand ‘arms’ has had a profound effect on the resulting copper(II) coordination environments (square pyramidal and octahedral in the analogous methylene linked complexes **A** and **B**, respectively³) as well as on the molecular architecture of the product formed in the absence of added base (the analogous methylene linked complex **A** is a dimer³ not a tetramer).

A nickel(II) [2 × 2] grid-type complex [Ni^{II}₄(HL^{Et})₄](BF₄)₄ (**5**) has been obtained by the 1 : 1 reaction of ligand and Ni(BF₄)₂·6H₂O, employing one equivalent of base. In contrast to the copper chemistry described above, no defined product could be isolated in the absence of added base. In complex **5** the monodeprotonated ligands (HL^{Et})⁻ act as bis-terdentate chelates, resulting in distorted N₆ octahedral coordination spheres about the nickel(II) ions.

Weak antiferromagnetic spin coupling has been observed for all three tetranuclear complexes **3–5**. For the copper(II) complexes, the magnetic susceptibility measurements have been used to establish the energies and multiplicities of the spin states. A spin singlet state ($S = 0$) is lowest in both cases, with a spin quintet state ($S = 2$) highest at energies of 13.4 cm⁻¹ and 18.12 cm⁻¹ for **3**·4H₂O and **4** respectively. The X-band EPR spectra of polycrystalline powders of the copper(II) complexes show evidence for exchange interactions consistent with the J values obtained from the magnetic susceptibility measurements. At temperatures below 4 K, the EPR signals for these complexes are primarily due to transitions within the lowest lying triplet state. For **4**, the apparent g values of $g_{\parallel} = 2.05$ and $g_{\perp} = 2.15$ can be explained as resulting from the alignment of the g matrix axes of the individual copper(II) ions and intramolecular exchange between the copper(II) ions of the square. Due to solute aggregation and disintegration of the complexes in solution, frozen solution spectra are unable to confirm the relative roles of inter- and intra-molecular exchange. However, the g values of the individual ions are consistent with the expected $d_{x^2-y^2}$ ground state for five-coordinate copper(II) in an approximately square pyramidal configuration.

Experimental

General

The magnetic susceptibility measurements were carried out using a Quantum Design MPMS5 Squid Magnetometer as described previously.³¹ Continuous wave (CW) EPR spectra were obtained with a Bruker ESP380FT/CW X-band spectrometer at Monash University. A standard rectangular TE₁₀₂ cavity was used with a Bruker nitrogen gas flow system for temperatures between 295 K and 120 K and with a quartz finger dewar for measurements at 77 K. Measurements at temperatures below 77 K down to 2.3 K were performed with an ER4118 cylindrical cavity and an Oxford Instruments CF935 cryostat. The temperature was calibrated against a germanium thermometer, using a carbon resistor as a transfer standard. The microwave frequency was measured with an EIP Microwave 548A frequency counter and the *g* values determined with reference to the F⁺ line in CaO (2.0001 ± 0.0001).³² Spectrum simulations used the SOPHE software described by Hanson and co-workers.³³ The potentiometric titrations of H₂L^{Me} and H₂L^{Et} were conducted in aqueous solutions with the addition of known amounts of standard 0.1 M HCl. Electrode potentials were measured using a high-precision Metrohm pH meter in mV mode with a resolution of 0.1 mV. Titrant (CO₂-free 0.1 M NaOH) was introduced manually for each point using a Metrohm digital burette. Titrations were carried out in the presence of 0.1 M NaClO₄ as an inert electrolyte. For each point the potential reading

E was taken when variations over 1–2 min were no greater than the 0.1 mV resolution of the pH meter. About 50 titration points were taken for each case. Both ligands were titrated in duplicate. The results of the titrations were processed using a custom computer application to calculate the required p*K*_a values.

X-Ray crystallography

Single crystal X-ray data were collected with a Bruker SMART CCD area detector diffractometer ($\lambda = 0.71073 \text{ \AA}$). The structures were solved by direct methods using SHELXS-97³⁴ and refined against *F*² using full-matrix least-squares techniques with SHELXL-97.³⁵ A summary of the crystallographic data and refinement parameters for H₂L^{Et}, 3·3MeCN·0.5H₂O, **4** and 5·10MeCN is given in Table 4.

CCDC reference numbers 296868 (**4**), 296869 (3·3MeCN·0.5H₂O), 296870 (H₂L^{Et}) and 296871 (5·10MeCN).

For crystallographic data in CIF or other electronic format see DOI: 10.1039/b614796h

Syntheses

Dimethyl pyrazine-2,3-dicarboxylate (2). Solid KMnO₄ (174 g, 1.10 mol) was slowly added to a solution of quinoxaline (24.0 g, 184 mmol) in H₂O (2 L) at 80–90 °C. The resulting mixture was maintained at this temperature for 1 h, before it was allowed to stir at RT for another 8 h. Then EtOH (40 mL) was added to

Table 4 Crystallographic data for H₂L^{Et} and the tetranuclear complexes 3·3MeCN·0.5H₂O, **4** and 5·10MeCN

	H ₂ L ^{Et}	3·3MeCN·0.5H ₂ O	4 ^a	5·10MeCN
Empirical formula	C ₂₀ H ₂₀ N ₆ O ₂	C _{21.5} H ₂₂ B _{1.5} CuF ₆ N _{6.75} O _{2.13}	C ₈₀ H ₇₆ B ₄ Cu ₄ F ₁₆ N ₂₄ O ₈	C ₁₀₀ H ₁₀₆ B ₄ F ₁₆ N ₃₄ Ni ₄ O ₈
<i>M</i> _r /g mol ⁻¹	376.42	602.71	2103.04	1912.12
<i>T</i> /K	83(2)	150(2)	168(2)	150(2)
Crystal system	Monoclinic	Triclinic	Tetragonal	Triclinic
Space group	<i>P</i> 2 ₁ / <i>n</i>	<i>P</i> $\bar{1}$	<i>I</i> $\bar{4}$	<i>P</i> $\bar{1}$
<i>a</i> /Å	5.0400(2)	13.9483(2)	16.152(3)	21.7134(3)
<i>b</i> /Å	20.6432(6)	14.1741(2)	16.152(3)	21.8434(3)
<i>c</i> /Å	17.8496(2)	26.0046(2)	17.855(8)	26.24680(10)
<i>a</i> /°	90	82.3380(10)	90	108.8230(10)
<i>β</i> /°	93.204(2)	86.1350(10)	90	103.0400(10)
<i>γ</i> /°	90	87.7230(10)	90	90.7210(10)
<i>V</i> /Å ³	1854.20(9)	5081.28(11)	4658(2)	11429.8(2)
<i>Z</i>	4	8	2	4
ρ_{calcd} /g cm ⁻³	1.348	1.576	1.499	1.449
μ /mm ⁻¹	0.092	0.939	0.999	0.744
<i>F</i> (000)	792	2446	2136	5136
Crystal colour and shape	Colourless needle	Green prism	Aqua-green plate	Red-brown block
Crystal size/mm	0.26 × 0.06 × 0.05	0.40 × 0.22 × 0.20	0.37 × 0.31 × 0.11	0.40 × 0.20 × 0.10
θ range/°	1.51/25.69	0.79/25.11	5.11/24.69	2.72/24.71
<i>h</i> _{min} / <i>h</i> _{max}	−5/6	−16/16	−17/8	−25/24
<i>k</i> _{min} / <i>k</i> _{max}	−25/24	−16/16	−18/18	−25/24
<i>l</i> _{min} / <i>l</i> _{max}	−20/21	0/30	−20/20	0/30
Reflections collected	10187	43733	9277	93504
Independent reflections	3494 [<i>R</i> _{int} = 0.0765]	17828 [<i>R</i> _{int} = 0.0331]	3910 [<i>R</i> _{int} = 0.0883]	38305 [<i>R</i> _{int} = 0.0996]
Completeness to θ (%)	99.2	98.5	98.9	98.3
Data/restraints/parameters	3494/0/261	17828/339/1480	3910/12/195	38305/0/2270
GOF on <i>F</i> ²	1.063	1.049	0.859	0.750
Final <i>R</i> indices [<i>I</i> > 2 σ (<i>I</i>)]	<i>R</i> 1 = 0.0604, <i>wR</i> 2 = 0.1066	<i>R</i> 1 = 0.0673, <i>wR</i> 2 = 0.1976	<i>R</i> 1 = 0.0613, <i>wR</i> 2 = 0.1286	<i>R</i> 1 = 0.0629, <i>wR</i> 2 = 0.1392
<i>R</i> indices (all data)	<i>R</i> 1 = 0.1226, <i>wR</i> 2 = 0.1315	<i>R</i> 1 = 0.0840, <i>wR</i> 2 = 0.2126	<i>R</i> 1 = 0.1252, <i>wR</i> 2 = 0.1479	<i>R</i> 1 = 0.1484, <i>wR</i> 2 = 0.1629
Largest diff. max, min/e Å ⁻³	0.256, −0.279	2.101, −0.968	0.281, −0.373	0.485, −0.310

^a The structure of **4** has disordered solvate and anion species that are not included in the structural model but were taken care of with SQUEEZE (see the CIF file for more details).

destroy excess KMnO_4 and the resulting mixture was filtered. The remaining MnO_2 cake was extracted with H_2O (5×400 mL). The combined aqueous solutions were reduced in volume (to approx. 300 ml) under reduced pressure, then conc. HCl (90 mL) was added and the resulting pale yellow suspension was stirred at RT for 1 h. Removal of the solvent under reduced pressure gave a pale yellow solid, which was taken up in MeOH (250 mL) and treated with SOCl_2 (10 mL). The suspension was refluxed for 5 h, was allowed to cool to RT and was then filtered. The remaining colourless solid was washed with MeOH (3×50 mL) and the combined filtrates were evaporated to dryness under reduced pressure. The resulting orange solid was taken up in Et_2O (100 mL) and the suspension was filtered. The remaining solid was extracted with Et_2O (5×100 mL). The filtrates were combined. Removal of the solvent under reduced pressure gave 32.8 g (91%) of compound **2** in the form of an analytically pure colourless crystalline material; mp: 52–55 °C. Elemental analysis (%) calcd for $\text{C}_8\text{H}_8\text{N}_2\text{O}_4$ (196.16 g mol^{-1}): C 48.98, H 4.11, N 14.28; found: C 48.73, H 3.99, N 14.28. TLC (SiO_2 , CH_2Cl_2 –10% MeOH): $R_f = 0.80$. ^1H NMR (300 MHz, CDCl_3): δ (ppm) = 8.54 (s, 2 H, 2 \times *pzH*), 3.70 (s, 6 H, 2 \times CH_3). $^{13}\text{C}\{^1\text{H}\}$ NMR (75 MHz, CDCl_3): δ (ppm) = 164.0 (CO_2), 145.3 (*pzCO*), 144.0 (*pzH*), 52.8 (CH_3).

***N,N'*-Bis[2-(2-pyridyl)ethyl]pyrazine-2,3-dicarboxamide ($\text{H}_2\text{L}^{\text{Et}}$).** A solution of compound **2** (2.00 g, 10.2 mmol) and 2-(2-aminoethyl)pyridine (2.49 g, 20.4 mmol) in MeOH (20 mL) was maintained at 80–90 °C for 5 h in an open flask, allowing the MeOH formed in the reaction to distil off and was then allowed to cool to RT. Removal of the remaining methanol under reduced pressure gave the crude product as a pale brown foamy solid in quantitative yield. Redissolution of the crude product in CH_2Cl_2 – Me_2CO 2 : 1 (50 mL), reduction of the solvent under reduced pressure (to approx. 10 mL) and filtration of the resulting colourless solid gave 3.22 g (83%) of analytically pure $\text{H}_2\text{L}^{\text{Et}}$ in the form of a colourless crystalline material; mp: 130–133 °C. Elemental analysis (%) calcd for $\text{C}_{20}\text{H}_{20}\text{N}_6\text{O}_2$ (376.42 g mol^{-1}): C 63.82, H 5.36, N 22.33; found: C 63.78, H 5.37, N 22.35. TLC (SiO_2 , CH_2Cl_2 –10% MeOH): $R_f = 0.38$. ^1H NMR (300 MHz, CDCl_3): δ (ppm) = 8.58 (s, 2 H, 2 \times *pzH*), 8.51 (ddd, $^3J_{6,5} = 4.9$ Hz, $^4J_{6,4} = 1.7$ Hz, $^5J_{6,3} = 0.9$ Hz, 2 H, 2 \times 6-*pyH*), 7.83 (s, 2 H, 2 \times *NH*), 7.61 (dt, $^3J_{4,5} = ^3J_{4,3} = 7.6$ Hz, $^4J_{4,6} = 1.7$ Hz, 2 H, 2 \times 4-*pyH*), 7.20 (d, $J = 7.8$ Hz, 2 H, 2 \times 3-*pyH*), 7.13 (ddd, $^3J_{5,4} = 7.6$ Hz, $^3J_{5,6} = 4.9$ Hz, $^4J_{5,3} = 1.1$ Hz, 2 H, 2 \times 5-*pyH*), 3.91 (q, $J = 6.2$ Hz, 4 H, 2 \times NHCH_2), 3.14 (t, $J = 6.5$ Hz, 4 H, 2 \times pyCH_2). $^{13}\text{C}\{^1\text{H}\}$ NMR (75 MHz, CDCl_3): δ (ppm) = 164.5 (CO), 159.5 (2-*py*), 149.3 (6-*py*), 147.1 (*pzCO*), 144.0 (*pzH*), 136.6 (4-*py*), 123.6 (3-*py*), 121.6 (5-*py*), 39.1 (NHCH_2), 36.9 (pyCH_2). IR (KBr, disk): $\bar{\nu}$ (cm^{-1}) = 3410, 3300, 3076, 3010, 2939, 2981, 1674, 1651, 1590, 1560, 1541, 1509, 1474, 1450, 1433, 1366, 1314, 1297, 1275, 1216, 1192, 1160, 1153, 1119, 1074, 1052, 1023, 1006, 991, 886, 774, 761, 749, 650, 612, 567, 511, 445. Single crystals of $\text{H}_2\text{L}^{\text{Et}}$ suitable for an X-ray crystal structure determination were obtained by recrystallisation from Me_2CO .

$[\text{Cu}^{\text{II}}_4(\text{H}_2\text{L}^{\text{Et}})_2(\text{HL}^{\text{Et}})_2](\text{BF}_4)_6$ (3**).** A solution of ligand $\text{H}_2\text{L}^{\text{Et}}$ (75.3 mg, 200 μmol) in MeCN (10 mL) was treated with a solution of $\text{Cu}(\text{BF}_4)_2 \cdot 4\text{H}_2\text{O}$ (61.8 mg, 200 μmol) in MeCN (5 mL). Vapour diffusion of Et_2O into the navy blue reaction mixture afforded 108 mg (88%) of compound **3**· $4\text{H}_2\text{O}$ in the form of turquoise-green feathery crystals. Elemental analysis (%) calcd

for $[\text{Cu}^{\text{II}}_4(\text{H}_2\text{L}^{\text{Et}})_2(\text{HL}^{\text{Et}})_2](\text{BF}_4)_6 \cdot 4\text{H}_2\text{O}$, $\text{C}_{80}\text{H}_{86}\text{B}_6\text{N}_{24}\text{O}_{12}\text{F}_{24}\text{Cu}_4$ (2350.72 g mol^{-1}): C 40.88, H 3.69, N 14.30; found: C 40.82, H 3.71, N 14.58. IR (KBr, disk): $\bar{\nu}$ (cm^{-1}) = 3422, 3076, 2924, 2854, 1636, 1607, 1569, 1542, 1484, 1446, 1423, 1376, 1338, 1310, 1253, 1226, 1132, 1083, 1062, 1037, 904, 870, 770, 745, 681, 650, 626, 591, 576, 521. ESI-MS (MeCN): m/z (fragment) = 438.0 ($[\text{Cu}^{\text{II}}(\text{HL}^{\text{Et}})]^+$), 377.1 ($[\text{H}_3\text{L}^{\text{Et}}]^{2+}$), 189.3 ($[\text{H}_4\text{L}^{\text{Et}}]^{2+}$). UV/Vis/NIR (MeCN): λ_{max} (ϵ) = 262 (87300), 622 nm (434 $\text{M}^{-1} \text{cm}^{-1}$). $A_m(\text{MeCN}) = 768 \Omega^{-1} \text{cm}^2 \text{mol}^{-1}$. Single crystals of **3**· 3MeCN · $0.5\text{H}_2\text{O}$ suitable for an X-ray crystal structure determination were obtained by vapour diffusion of Et_2O into a dilute (1 mg mL^{-1}) solution of compound **3**· $4\text{H}_2\text{O}$ in MeCN .

$[\text{Cu}^{\text{II}}_4(\text{HL}^{\text{Et}})_4](\text{BF}_4)_4$ (4**).** A solution of ligand $\text{H}_2\text{L}^{\text{Et}}$ (400 mg, 1.06 mmol) in MeCN (60 mL) was treated with a solution of $\text{Cu}(\text{BF}_4)_2 \cdot 4\text{H}_2\text{O}$ (329 mg, 1.06 mmol) in MeCN (10 mL) and a solution of NEt_3 (107 mg, 1.06 mmol) in MeCN (5 mL). Toluene (220 mL) was added and a dark bottle green solid precipitated. Filtration of the solid gave 480 mg (86%) of compound **4** in the form of a bottle green amorphous solid. Elemental analysis (%) calcd for $[\text{Cu}^{\text{II}}_4(\text{HL}^{\text{Et}})_4](\text{BF}_4)_4$, $\text{C}_{80}\text{H}_{76}\text{B}_4\text{N}_{24}\text{O}_8\text{F}_{16}\text{Cu}_4$ (2103.04 g mol^{-1}): C 45.69, H 3.64, N 15.98; found: C 45.36, H 3.63, N 15.77. IR (KBr, disk): $\bar{\nu}$ (cm^{-1}) = 3417, 3074, 2924, 2838, 1636, 1569, 1539, 1484, 1446, 1422, 1373, 1332, 1310, 1250, 1225, 1133, 1083, 1060, 881, 771, 595, 520. ESI-MS (MeCN): m/z (fragment) = 483.9, 438.0 ($[\text{Cu}^{\text{II}}(\text{HL}^{\text{Et}})]^+$), 377.1 ($[\text{H}_3\text{L}^{\text{Et}}]^{2+}$), 189.3 ($[\text{H}_4\text{L}^{\text{Et}}]^{2+}$). UV/Vis/NIR (MeCN): λ_{max} (ϵ) = 263 (73200), 656 (603), 803 nm (shoulder) (356 $\text{M}^{-1} \text{cm}^{-1}$). $A_m(\text{MeCN}) = 531 \Omega^{-1} \text{cm}^2 \text{mol}^{-1}$. Single crystals of complex **4** suitable for an X-ray crystal structure determination were obtained by vapour diffusion of Et_2O into a solution of the compound in MeCN .

$[\text{Ni}^{\text{II}}_4(\text{HL}^{\text{Et}})_4](\text{BF}_4)_4$ (5**).** A solution of $\text{H}_2\text{L}^{\text{Et}}$ (80.2 mg, 213 μmol) in MeCN (7 mL) was treated with a solution of $\text{Ni}(\text{BF}_4)_2 \cdot 6\text{H}_2\text{O}$ (72.5 mg, 213 μmol) in MeCN (5 mL) and a solution of NEt_3 (21.6 mg, 213 μmol) in MeCN (4 mL). Vapour diffusion of Et_2O into the red-brown reaction mixture afforded 72.4 mg (60%) of compound **5**· $10\text{H}_2\text{O}$ in the form of dark red-brown crystals. Elemental analysis (%) calcd for $[\text{Ni}^{\text{II}}_4(\text{HL}^{\text{Et}})_4](\text{BF}_4)_4 \cdot 10\text{H}_2\text{O}$, $\text{C}_{80}\text{H}_{96}\text{B}_4\text{N}_{24}\text{O}_{18}\text{F}_{16}\text{Ni}_4$ (2263.77 g mol^{-1}): C 42.45, H 4.27, N 14.85; found: C 42.53, H 3.91, N 14.70. IR (KBr, disk): $\bar{\nu}$ (cm^{-1}) = 3419, 1652, 1605, 1562, 1464, 1443, 1413, 1371, 1346, 1307, 1238, 1145, 1083, 1063, 1031, 976, 898, 847, 769, 735, 680, 643, 588, 521. ESI-MS (MeCN): m/z (fragment) = 997.0 ($[\text{Ni}^{\text{II}}_4(\text{H}_2\text{L}^{\text{Et}})(\text{HL}^{\text{Et}})_3](\text{BF}_4)_3^{2+}$), 973.0 ($[\text{Ni}^{\text{II}}_4(\text{H}_2\text{L}^{\text{Et}})_2(\text{HL}^{\text{Et}})_2(\text{H}_2\text{O})_2](\text{BF}_4)_2^{2+}$), 953.1 ($[\text{Ni}^{\text{II}}_4(\text{HL}^{\text{Et}})_4](\text{BF}_4)_2^{2+}$), 909.2 ($[\text{Ni}^{\text{II}}_4(\text{HL}^{\text{Et}})_3(\text{L}^{\text{Et}})](\text{BF}_4)_3^{2+}$), 683.8 ($[\text{Ni}^{\text{II}}_4(\text{H}_2\text{L}^{\text{Et}})_2(\text{HL}^{\text{Et}})_2(\text{H}_2\text{O})_3](\text{BF}_4)_3^{3+}$), 653.3, 620.0 ($[\text{Ni}^{\text{II}}\text{Ni}^{\text{I}}_3(\text{H}_2\text{L}^{\text{Et}})_3(\text{HL}^{\text{Et}})_2(\text{H}_2\text{O})_2](\text{BF}_4)_3^{3+}$), 606.7 ($[\text{Ni}^{\text{II}}_4(\text{HL}^{\text{Et}})_4](\text{BF}_4)_3^{3+}$), 598.4, 577.5 ($[\text{Ni}^{\text{II}}_4(\text{HL}^{\text{Et}})_3(\text{L}^{\text{Et}})]^{3+}$), 433.0 ($[\text{Ni}^{\text{II}}_4(\text{HL}^{\text{Et}})_4]^{4+}$), 377.2 ($[\text{H}_3\text{L}^{\text{Et}}]^{2+}$), 189.4 ($[\text{H}_4\text{L}^{\text{Et}}]^{2+}$). UV/Vis/NIR (MeCN): λ_{max} (ϵ) = 260 (50000), 853 nm (89 $\text{M}^{-1} \text{cm}^{-1}$). $A_m(\text{MeCN}) = 454 \Omega^{-1} \text{cm}^2 \text{mol}^{-1}$. Single crystals of complex **5**· 10MeCN suitable for an X-ray crystal structure determination were obtained by vapour diffusion of Et_2O into a solution of compound **5**· $10\text{H}_2\text{O}$ in MeCN .

Acknowledgements

This work was supported by grants from the University of Otago (Postgraduate Scholarship to JK and a Bridging Grant),

the Marsden Fund (Royal Society of New Zealand), and the Australian Research Council (Discovery Grant). JFB and JRP acknowledge support from the School of Physics, Monash University. JK thanks Dr M. H. Klingele (University of Otago) for many helpful discussions. The authors thank Prof. W. T. Robinson and Dr J. Wikaira (University of Canterbury) and Prof. G. Clark and T. Groutso (University of Auckland) for the X-ray data collections, Prof. M. A. Hitchman (University of Tasmania) and Dr E. J. L. McInnes (University of Manchester) for helpful discussions and calculations, and S. S. Iremonger (University of Otago) for practical support.

References

- 1 M. Ruben, J. Rojo, F. J. Romero-Salguero, L. H. Uppadine and J.-M. Lehn, *Angew. Chem., Int. Ed.*, 2004, **43**, 3644; L. K. Thompson, O. Waldmann and Z. Xu, *Coord. Chem. Rev.*, 2005, **249**, 2677.
- 2 J. R. Nitschke, M. Hutin and G. Bernardinelli, *Angew. Chem., Int. Ed.*, 2004, **43**, 6724; S. Brooker, S. J. Hay and P. G. Plieger, *Angew. Chem., Int. Ed.*, 2000, **39**, 1968; Y. Lan, D. K. Kennepohl, B. Moubaraki, K. S. Murray, J. D. Cashion, G. B. Jameson and S. Brooker, *Chem.–Eur. J.*, 2003, **9**, 3772; J. Hausmann and S. Brooker, *Chem. Commun.*, 2004, 1530.
- 3 J. Hausmann, G. B. Jameson and S. Brooker, *Chem. Commun.*, 2003, 2992.
- 4 D. S. Cati, J. Ribas, J. Ribas-Arino and H. Stoeckli-Evans, *Inorg. Chem.*, 2004, **43**, 1021.
- 5 See for example: D. L. Caulder, C. Bruckner, R. E. Powers, S. König, T. N. Parac, J. A. Leary and K. N. Raymond, *J. Am. Chem. Soc.*, 2001, **123**, 8923.
- 6 See for example: J. R. Nitschke and J.-M. Lehn, *Proc. Natl. Acad. Sci. U. S. A.*, 2003, **100**, 11970; J. R. Nitschke, D. Schultz, G. Bernardinelli and D. Gérard, *J. Am. Chem. Soc.*, 2004, **126**, 16538.
- 7 D. S. Cati and H. Stoeckli-Evans, *Acta Crystallogr., Sect. E*, 2004, **60**, o210.
- 8 E. B. Fleischer and M. B. Lawson, *Inorg. Chem.*, 1972, **11**, 2772; I. Mallik and S. Mallik, *Synlett*, 1996, 734.
- 9 E. B. Fleischer, D. Jeter and R. Florian, *Inorg. Chem.*, 1974, **13**, 1042.
- 10 S. Gabriel and A. Sonn, *Ber. Dtsch. Chem. Ges.*, 1907, **40**, 4850; R. G. Jones and K. C. McLaughlin, *Org. Synth.*, 1950, **30**, 87.
- 11 P. W. Baures, J. R. Rush, A. V. D. Wiznycia, J. B. A. Helfrich and A. M. Beatty, *Cryst. Growth Des.*, 2002, **2**, 653.
- 12 K. Nonoyama, W. Mori and M. Nonoyama, *Polyhedron*, 1994, **13**, 891.
- 13 A. Braibanti, F. Dallavalle, G. Mori and B. Veroni, *Talanta*, 1982, **29**, 725.
- 14 G. Aylward and T. Findlay, *SI Chemical Data*, John Wiley & Sons, Singapore, 1998.
- 15 B. C. Challis and J. A. Challis, *Comprehensive Organic Chemistry*, Pergamon Press, Liverpool, 1979.
- 16 A. W. Addison, T. N. Rao, J. Reedijk, J. van Rijn and G. C. Verschoor, *J. Chem. Soc., Dalton Trans.*, 1984, 1349.
- 17 D. S. Cati and H. Stoeckli-Evans, *Acta Crystallogr., Sect. E*, 2004, **60**, m180; T. Yano, R. Tanaka, T. Nishioka, I. Kinoshita, K. Isobe, L. J. Wright and T. J. Collins, *Chem. Commun.*, 2002, 1396.
- 18 P. van der Sluis and A. L. Spek, *Acta Crystallogr., Sect. A*, 1990, **46**, 194.
- 19 W. E. Hatfield and G. W. Inman, Jr., *Inorg. Chem.*, 1969, **8**, 1376.
- 20 K. S. Murray, *Adv. Inorg. Chem.*, 1995, **43**, 261.
- 21 J. Ribas, M. Montserrat, T. Costa and X. Solans, *Inorg. Chem.*, 1993, **32**, 695.
- 22 B. J. Kennedy, K. S. Murray, M. A. Hitchman and G. L. Rowbottom, *J. Chem. Soc., Dalton Trans.*, 1987, 825.
- 23 R. W. Jotham and S. F. A. Kettle, *Inorg. Chim. Acta*, 1970, **4**, 145. The same expressions are obtained after some algebraic manipulation from: J. W. Hall, W. E. Estes, E. D. Estes, R. P. Scaringe and W. E. Hatfield, *Inorg. Chem.*, 1977, **16**, 1572.
- 24 A. Abragam and B. Bleaney, *Electron paramagnetic resonance of transition ions*, Clarendon Press, Oxford, 1970, p. 456 and p. 459; M. A. Halcrow, *Dalton Trans.*, 2003, 4375.
- 25 N. K. Solanki, M. A. Leech, E. J. L. McInnes, F. E. Mabbs, J. A. K. Howard, C. A. Kilner, J. M. Rawson and M. A. Halcrow, *J. Chem. Soc., Dalton Trans.*, 2002, 1295.
- 26 A. Bencini and D. Gatteschi, *EPR of Exchange Coupled Systems*, Springer-Verlag, Berlin, 1990.
- 27 A. Bencini, D. Gatteschi, C. Zanchini, J. G. Haasnoot, R. Prins and J. Reedijk, *J. Am. Chem. Soc.*, 1987, **109**, 2926; P. Chaudhuri, I. Karpenstein, M. Winter, M. Lengen, C. Butzlaff, E. Bill, A. X. Trautwein, U. Florke and H. J. Haupt, *Inorg. Chem.*, 1993, **32**, 888.
- 28 K. L. V. Mann, E. Psillakis, J. C. Jeffery, L. H. Rees, N. M. Harden, J. A. McCleverty, M. D. Ward, D. Gatteschi, F. Totti, F. E. Mabbs, E. J. L. McInnes, P. C. Riedi and G. M. Smith, *J. Chem. Soc., Dalton Trans.*, 1999, 339.
- 29 Z. G. Soos, K. T. McGregor, T. T. P. Cheung and A. J. Silverstein, *Phys. Rev. B*, 1977, **16**, 3036.
- 30 J. Peisach and W. E. Blumberg, *Arch. Biochem. Biophys.*, 1974, **165**, 691.
- 31 J. Klingele (née Hausmann), B. Moubaraki, K. S. Murray, J. F. Boas and S. Brooker, *Eur. J. Inorg. Chem.*, 2005, 1530.
- 32 J. E. Wertz, J. W. Orton and P. Auzins, *Discuss. Faraday Soc.*, 1961, **31**, 140.
- 33 G. R. Hanson, K. E. Gates, C. J. Noble, M. Griffin, A. Mitchell and S. Benson, *J. Inorg. Biochem.*, 2004, **98**, 903.
- 34 G. M. Sheldrick, *Acta Crystallogr., Sect. A*, 1990, **46**, 467; G. M. Sheldrick, *Methods Enzymol.*, 1997, **276**, 628.
- 35 G. M. Sheldrick and T. R. Schneider, *Methods Enzymol.*, 1997, **277**, 319.